DOPAMINE SENSING

WITH

CARBON NANOTUBES AND GRAPHITE ELECTRODES

By

Mesut Yilmaz

Thesis

Submitted to the Faculty of the Graduate School of

Vanderbilt University

in partial fulfillment of the requirements

for the degree of

MASTER OF SCIENCE

in

Electrical Engineering

August, 2011

Nashville, Tennessee

Approved:

Professor Weng Poo Kang

Professor Jimmy L. Davidson

To my family

ACKNOWLEDGEMENTS

First of all, I would like to thank my academic advisor Professor Weng Poo Kang for his assistance, guidance and encouragement through my studies at Vanderbilt University. I would also like to thank to Supil Raina for his advisory support.

Finally, I would like to thank to my dear parents and brother for their continuous and sincere support.

TABLE OF CONTENTS

Page

DEDICATION ii

ACKNOWLEDGEMENTS iii

ABSTRACT vi

LIST OF FIGURES vii

Chapter

I. INTRODUCTION 1

1.1 Electrochemical Biosensor 1

1.2 Carbon Nanotubes and Graphite 4

1.3 Electronic Properties of Carbon Nanotubes and Graphite 9

1.4 Cyclic Voltammogram (CV) 10

1.5 Objectives of Research 14

1.6 Organization of Thesis 15

II. GROWTH AND CHARACTERIZATION OF CNTs 16

2.1 Raman Spectra 18

III. IMPLEMENTATION OF CNT AND GRAPHITE FOR ELECTROCHEMICAL BIOSENSING OF DOPAMINE 21

IV. CONCLUSION 45

V. RECOMMENDATIONS 47

REFERENCES 48

ABSTRACT

The superior material properties of carbon nanotubes (CNTs) such as high aspect ratio, high surface area, superb mechanical properties, thermal and chemical stability have generated enormous research activities to push for their potential applications. This study focuses on the fabrication and characterization of CNTs synthesized by hot filament chemical vapor deposition and evaluates their use as electrochemical biosensor. The as grown CNTs were first characterized for their electrochemical behavior in ferrocyanide redox reaction using cyclic voltammetric analysis. Then, their use for dopamine detection was investigated. Well-established redox reaction current peaks for dopamine/o-quinone and the secondary redox reaction current peaks for leucodopominechrome/dopaminechrome were reproducibility observed with distinct redox current peak increments as a function of the bioanalyte concentration. These results were also confirmed by Cottrell and Nernst equations. In general, the results have demonstrated that CNTs are better than graphite as biosensor electrode for the detection of dopamine.

LIST OF FIGURES

Figure Page

1.1 Schematic diagram of an amperematic enzyme based electrochemical biosensor [5]..2

1.2 Honeycomb binding of sp^2 carbon atoms forms graphene [14]..5

1.3 Bonding structure of graphite. a) sp^2 bonding of carbon atoms, b) three graphene sheets overlaid to form graphite [13]..6

1.4 Schematic diagram of CNTs made of rolled graphene (graphite sheet) a) Single walled CNT, b) Multi-walled CNT [15]..7

1.5 Schematic diagram of graphite sheet and the chiral vector..8

1.6 Rolling hexagonal graphene sheets in different directions gives three types of SWCNTs: armchair, zigzag, and chiral [13]..9

1.7 Illustration of potential-time stimulation signal of the cyclic voltammetry [3]..10

1.8 Current vs. Potential in a cyclic voltammetric analysis of a reversible O + ne- $\rightleftharpoons$ R redox reaction [3]..12

2.1 SEM picture of CNTs on N^+ type Si wafer. 4 minute flow of methane (CH_4) yielded nearly 19µm long nanotubes..18

2.2 Raman spectra (Intensity vs. Wavenumber/Raman shift) of the MPCVD and thermal CVD grown CNTs [24]..20

3.1 Biosensing setup with three electrodes inside a glass cell. The electrodes are connected to faraday cage and a current amplifier system through wires..22

3.2 Voltage sweep curves of 1, 2, 3, 4, and 5mM $Fe(CN)_6^{4-}$ on graphite electrode at 100mV/s..25

3.3 Concentration versus current curves for the redox reactions obtained after the CV scan of ferrocyanide on graphite electrode at 100mV/s..26

3.4 5mM Ferrocyanide CV scans with the scan rates of 10, 50, 100, 200, and 500mv/s (from red to navy blue) where KCL background CV curves for the respective scan rates are subtracted..27

3.5 $\sqrt{SR}$ versus redox peak current of 5mM ferrocyanide on graphite electrode where SR refers to scan rate (10, 50, 100, 200, and 500mV/s)……..28

3.6 Concentration (1-5mM) versus current curves for the ferrocyanide redox reactions on CNT electrode, operating at a constant scan rate of 100mV/s. (a) CV curves, and (b) calibration curves…..……29

3.7 $\sqrt{SR}$ versus redox peak current of 5mM ferrocyanide on CNT electrode where SR refers to scan rate (10, 50, 100, 200, and 500mV/s). (a) CV curves, and (b) calibration curves……..31

3.8 Voltage sweep curve of 400µM dopamine on graphite at 100mV/s. Four separate redox peaks (labeled with numbers 1-4) can be seen……..34

3.9 Voltage sweep curves of 100, 200, 400, 600, and 800µM dopamine on graphite at 100mV/s……35

3.10 Concentration (100, 200, 400, 600, and 800µM) versus current curves for the redox reactions obtained after the CV scan of dopamine with graphite electrode at 100mV/s……..36

3.11 $\sqrt{SR}$ versus redox current peak height of 200µM dopamine on graphite electrode where SR refers to scan rate (10, 50, 100, 200, and 500mV/s) (a) CV curves, and (b) calibration curves……..37

3.12 Concentration (100, 200, 400, 600, and 800µM) versus current curves for the DA redox reactions at CNT electrode, operating at a constant scan rate of 100mV/s. (a) CV curves, and (b) calibration curves……..39

3.13 Comparison of concentration (100, 200, 400, 600, and 800µM) versus current curves for the redox reactions obtained after the CV scan of dopamine with CNT and graphite electrodes, separately at 100mV/s. Dashed and solid lines correspond to graphite and CNT working electrodes, sequentially……41

3.14 $\sqrt{SR}$ versus redox peak current of 200µM dopamine on CNT electrode where SR refers to scan rate (10, 50, 100, 200, and 500mV/s). (a) CV curves, and (b) calibration curves……..42

3.15 Comparison of $\sqrt{SR}$ versus redox peak current of 200µM dopamine with CNT and graphite electrodes, separately, where SR refers to scan rate (10, 50, 100, 200, and 500mV/s). Dashed and solid lines correspond to graphite and CNT working electrodes, sequentially……44

CHAPTER I

INTRODUCTION

1.1 Electrochemical Biosensor

The biosensor concept was initially proposed and created by Leland C. Clark Jr. . His first study was on oxygen detecting electrode in 1956. Later in 1962, Prof. Clark turned his inspiring efforts on making biosensor which was able to sense glucose using enzyme electrode [1]. Biosensors are analytical devices that are able to recognize biochemical information of an analyte's concentration or chemical structure and transform it into a logical signal [2]. Since they deal with biologically reactive compounds, biosensors are more specialized version of chemical sensors. Electrochemical biosensors are categorized into two types as affinity and enzymatic biosensors. Affinity biosensors employ DNA sequence, antibody or receptor protein along with transducer to bind target species and produce electrical signal [3, 4]. On the other hand, enzymatic biosensors use cells, enzymes or tissues for the recognition process. In the biosensor, transducer utilizes the recognition process to output electrical signal. Sensitivity of sensing depends on electrochemical reaction rate and concentration of the target compound. In Figure 1.1, a basic schematic structure of a biosensor is shown.

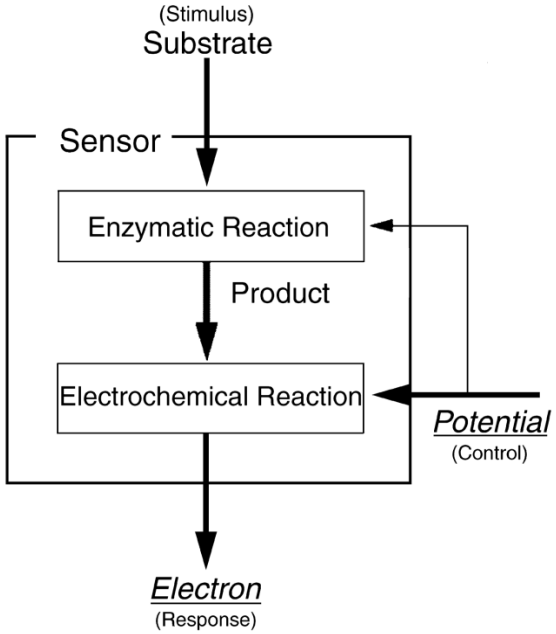

Figure 1.1: Schematic diagram of an amperematic enzyme based electrochemical biosensor [5].

Biosensors are usually equipped with magnetic, thermic, radioactive, optical or electrochemical energy conversion abilities. In medical applications, electrochemical biosensors are the most needed ones, which make use of a working electrode as physico-chemical transducer. They are mostly used in health care and pharmaceutical industries as well as environmental applications. This tendency for biosensing stems from the facts that they are inexpensive, simple to put to practical use, sensitive, fast, and responsive to many biochemical species.

Since 1962, attention to biosensors has been increasing as a research topic and commercialized medical devices. In Europe, Asia-Pacific and North America, many companies aimed at development and fabrication of biosensors were founded [6]. In

bio-sensing field, scientists have also shown keen interest to sense neurotransmitters, enzymes, proteins, DNA, cells, antibodies, tissues, nucleic acids and many other biological molecules and mechanisms.

As a catecholamine neurotransmitter, dopamine has a key physiological role in transmitting chemical signals out of the cells [7]. Mostly abbreviated as DA, dopamine is crucial for the sound working of cerebral functions, central nervous, renal, cardiovascular and hormonal systems. It also has an important role in detecting the emergence of Parkinson's disease, drug abuse, and HIV infection of some cells [8, 9, and 10]. In addition, dopamine is usually presented *in vivo* with other electroactive materials, and sometimes in very low concentrations; which make it harder to sense. Therefore, electrodes that are capable of sensing low concentrations of DA in human body, rapidly, accurately and reliably, are in great need. In means of dopamine sensing technique, cyclic voltammogram (CV) is very appropriate because DA is very responsive to CV when it is in electrochemical reaction.

Researchers have proposed and/or developed different types of electrodes for dopamine measurement. Some of them are made of gold, carbon nanotubes, carbon fiber, glassy carbon, graphite and diamond. In this work, vertical-aligned multi-walled carbon nanotubes were used to sense dopamine. Besides, electrochemical activity of DA was analyzed using cyclic voltammogram.

Recently, there is great interest of using nanotechnology approach for biosensor. Nanotechnology is an emerging science/technology about the understanding and

control of matter's structure in a scale of billionth of a meter. Since it mostly deals with the matter itself in the atomic scale, this makes nanotechnology applicable to many materials. According to Nalwa et al, nanostructured materials have many novel applications based on their fabrication and production techniques. The potential applications of nanotechnology have been demonstrated in many areas such as aerospace, batteries, automotive, optoelectronics, medicine, pharmacy, and other areas. [11] Among these, biomedical science takes the advantages of nano-scale structures for variety of applications such as biosensing, drug delivery, medical diagnostics, microelectromechanical systems (MEMS), bio-molecular patterning and so forth [12]. In this thesis, CNTs and graphite nanostructured material are used for DA detection.

1.2 Carbon Nanotubes and Graphite

Carbon nanotubes (CNTs) were first discovered in early 1990s by Sumia Iijima. They have remarkable mechanical and electrical properties. Since their first discovery, CNTs have gained much interest in material's science, electronics, computing, etc. Although CNTs are not widespread in mass production, their unique properties have made them arbiter in materials science for chemical and biological separation, purification and catalysis, energy storage (fuel cells, lithium battery), composites for filling, structural materials and coating. In devices' side, CNTs have shown promising applications for sensors, actuators, transistors, logic devices, and field emission

cathodes of x-ray instruments, displays, and other vacuum nanoelectronics. The most important benefits of CNTs for these applications are low cost, lightness, energy efficiency, high performance, and small size [13].

The electronic structure of CNTs consists of sp^2 hybridized carbon atoms (Fig. 1.3-a). The sp^2 orbited carbon atoms aligned in honeycomb lattice form graphene (Fig. 1.2), which is single-layer graphite.

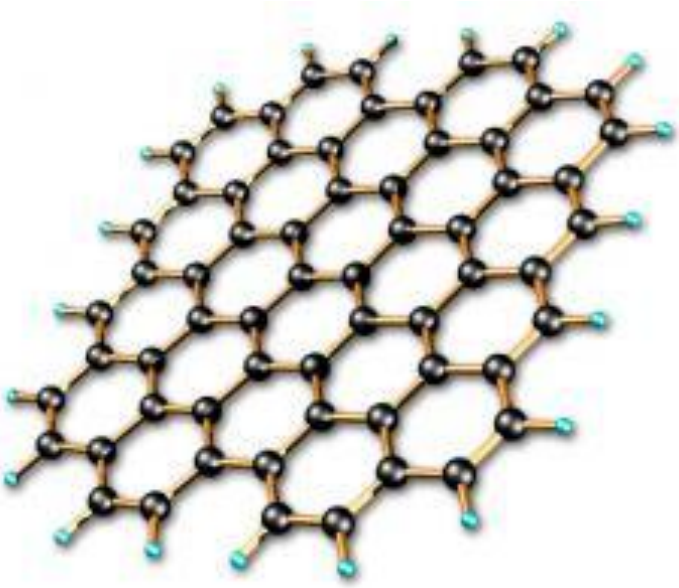

Figure 1.2: Honeycomb binding of sp^2 carbon atoms forms graphene [14].

On the other hand, graphite consists of multiple graphene sheets laid on top of each other (Fig. 1.3-b). Finally, CNTs are made of rolled graphite sheets. If one graphite sheet is rolled over, the shape is single-walled CNT (SWCNT) (Fig. 1.4-a), while rolling two or more sheets of graphite is yielding multi-walled CNTs (MWCNT) (Fig. 1.4-b).

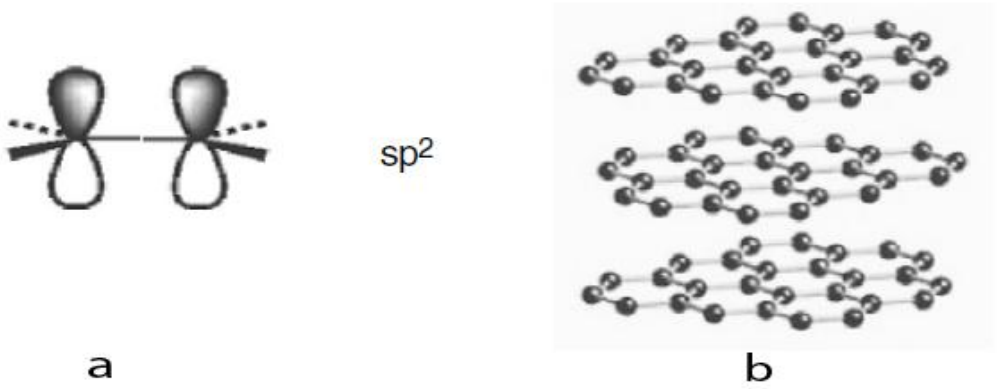

Figure 1.3: Bonding structure of graphite. a) sp^2 bonding of carbon atoms, b) three graphene sheets overlaid to form graphite [13].

Scientists define multi-walled CNTs as concentric and closed graphite tubes with many layers of graphite sheets separated from each other by ~ 0.34nm, and forming a center hole of 2 to 25nm diameter. In addition, single-walled CNTs are cylinders with a diameter of 1-2 nm [15].

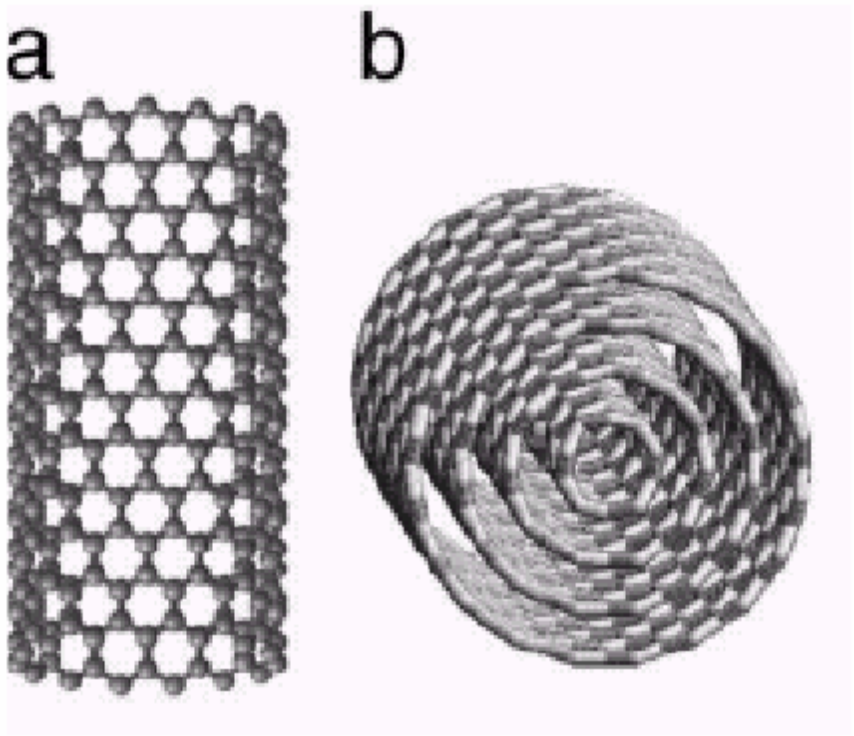

Figure 1.4: Schematic diagram of CNTs made of rolled graphene (graphite sheet) a) Single walled CNT, b) Multi-walled CNT [15].

Depending on its rolling directions, a carbon nanotube can be classified into three categories: armchair, zigzag, and chiral (Fig. 5). The explanation for this is as follows. By definition, graphene is rolled across a chiral vector (Fig. 1.5) defined as

$\vec{C}_h = n\vec{a}_1 + m\vec{a}_2$ .....(1),

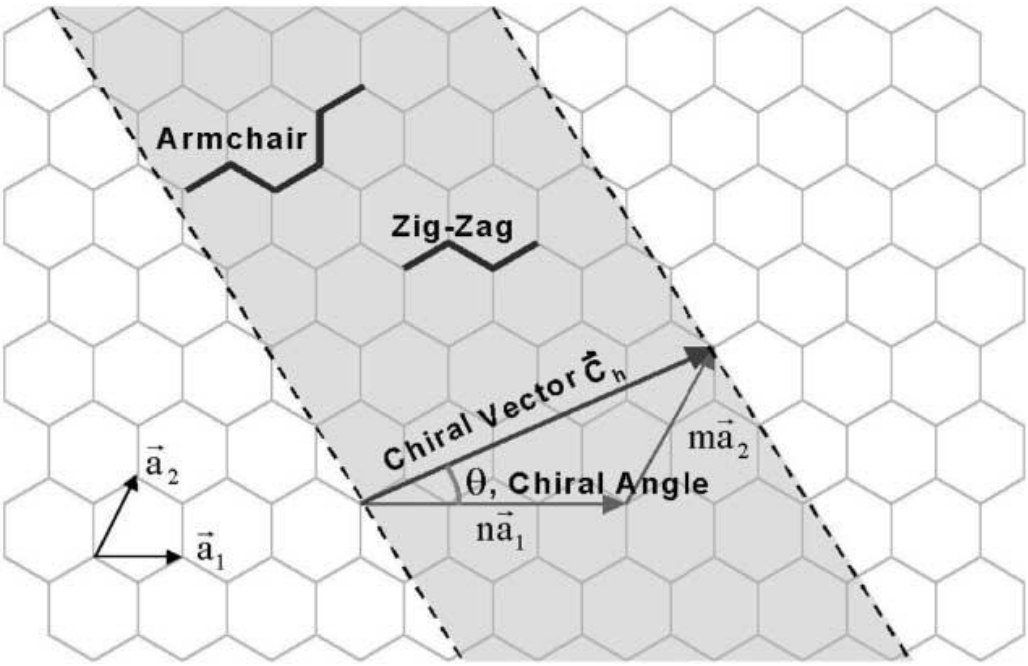

Figure 1.5: Schematic diagram of graphite sheet and the chiral vector.

where $\vec{a}_1$ and $\vec{a}_2$ are basis vectors, θ is the chiral angle, and carbon atoms are located at the vertices [15]. While employing Equation (1), taking m as zero and n as an integer value shapes zigzag nanotube, m=n shapes armchair nanotube, and $n > m > 0$ shapes chiral nanotube (Fig. 1.6)

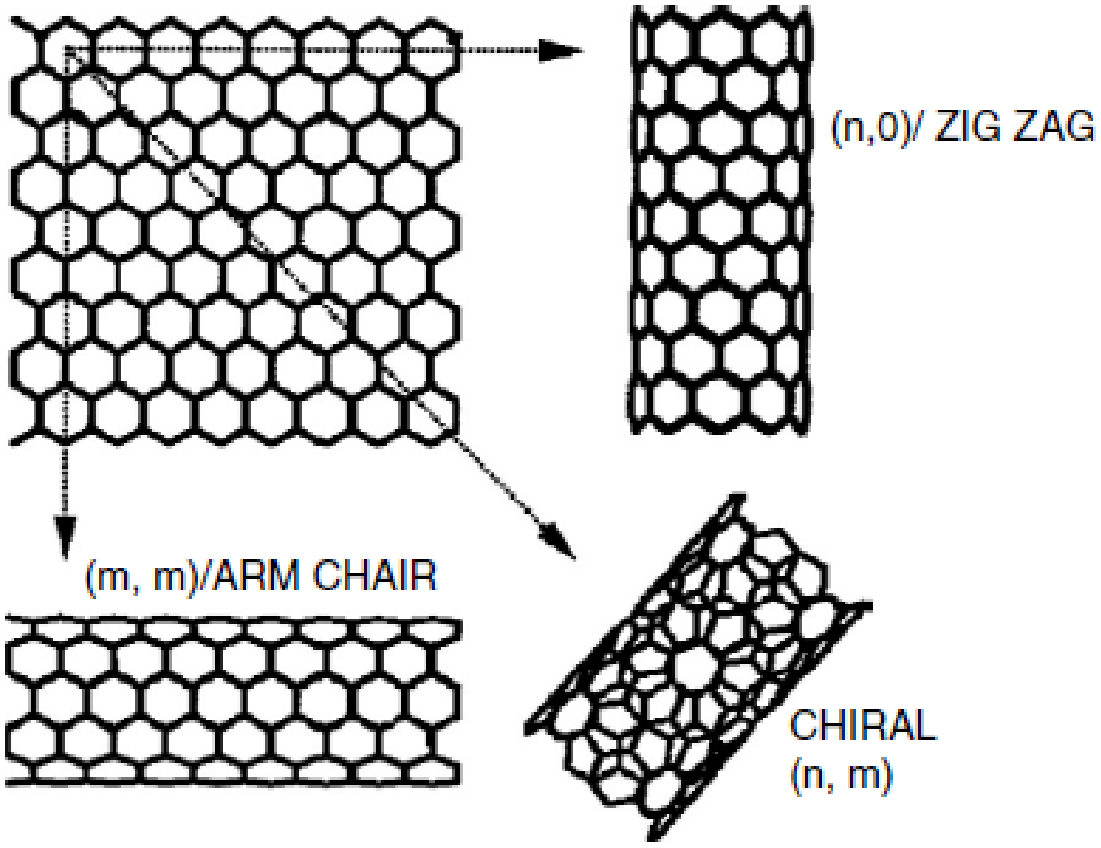

Figure 1.6: Rolling hexagonal graphene sheets in different directions gives three types of SWCNTs: armchair, zigzag, and chiral [13].

1.3 Electronic Properties of Carbon Nanotubes and Graphite

Electronic properties of nanotubes had much interest since their discovery. CNTs actually behave like quantum wires and this makes them have unique electronic specialties. Nanotubes' electrical properties rely on the n and m values of the chirality vector and thus, on the chirality and diameter. (m, n) indices determine SWCNTs to be either metal, semiconductor or small-gap semiconductor. If n=m, CNT is metallic [15]. Besides, n − m = 3 x integer equality makes CNTs have a very small energy band gap and

behave metallic (at room temperature). For the rest of n and m values, CNTs become semiconductor with a finite gap. Scientists have also proven that armchair nanotubes are metallic, whereas zigzag nanotubes are either semiconductor or metallic depending on their chiral angle and diameter [15].

1.4 Cyclic Voltammogram (CV)

Cyclic voltammetry is the mostly used technique for determining qualitative information about electrochemical reactions, and thus, for biosensors as well [3]. It comprises of ceaselessly scanning the potential of a stationary working electrode operating under a triangular potential waveform (Fig. 1.7).

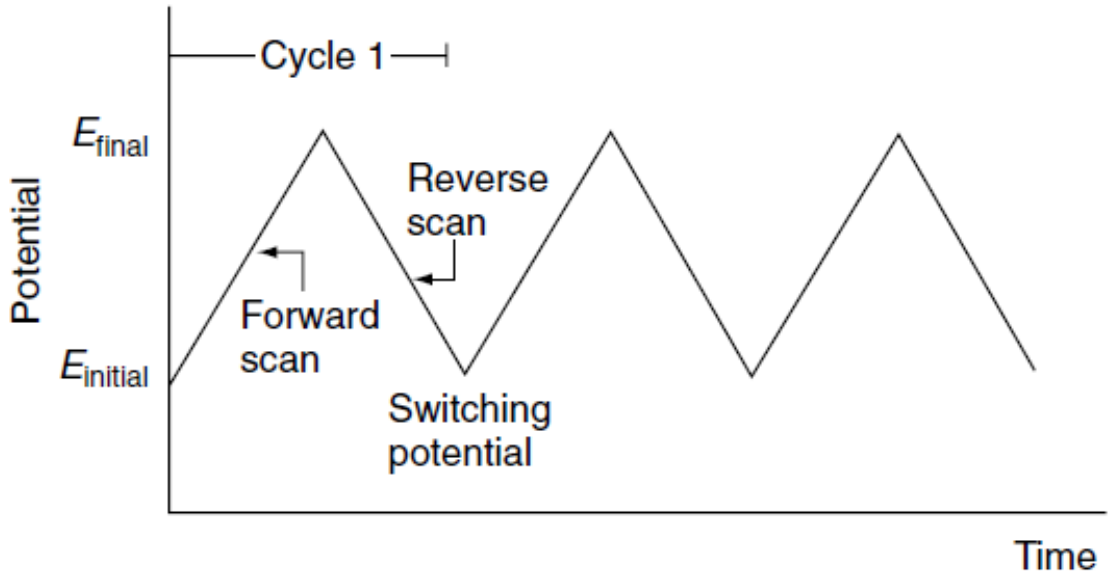

Figure 1.7: Illustration of potential-time stimulation signal of the cyclic voltammetry [3].

When the voltage in Figure 1.7 is applied to the working electrode, two electrochemical reactions take place: oxidation and reduction. Oxidation, which is indicated in the leftwards direction of electrochemical reaction stated in (2), is the loss of electron(s).

$$O + ne^- \rightleftharpoons R \quad \text{.....(2)}$$

On the other hand, reduction is the gain of electron(s) and it occurs in the forward scan as described in Fig. 1.8. The resulting currents seen on the triangular potential scan are cathodic for the forward scan, and anodic for the reverse scan.

In the cyclic voltammogram, current amplitude is affected by the chemical reaction rate, voltage applied, and the analyte. In addition, current peak is formulated with Cottrell Equation

$$i_p = (2.69 \times 10^5) n^{3/2} A C D^{1/2} v^{1/2} \quad \text{.....(3)}$$

where *n* is the number of electrons, *A* the electrode area (in cm^2), *C* the concentration in ($mole/cm^2$), D the diffusion coefficient, and v the potential scan rate (in V/s) [3]. In a fixed experimental setup which has a stagnant solution; the electrode area, concentration of the species, and the number of electrons remain constant. As a result, square root of scan rate directly changes the current peak during most CV implementation.

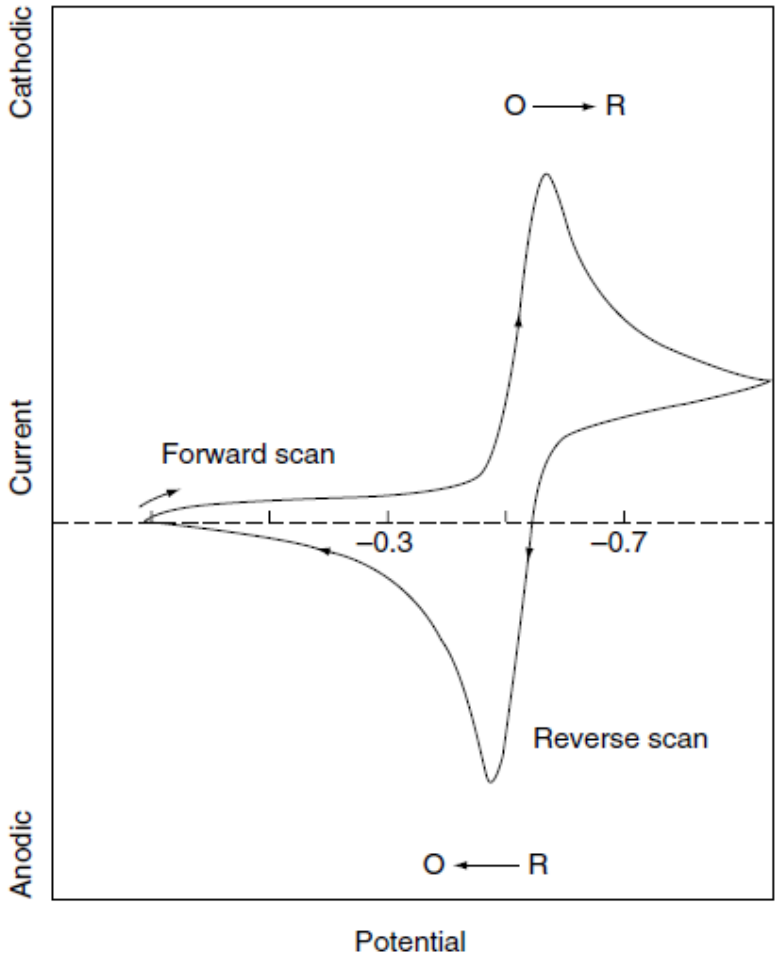

Figure 1.8: Current vs. Potential in a cyclic voltammetric analysis of a reversible $O + ne^- \rightleftharpoons R$ redox reaction [3].

Before any voltage is applied to the reference electrode, there is equilibrium at the working electrode surface. In this condition, two forces balance each other: diffusion and the electrical force. That is, initial diffusion of ions into cell creates an electric field, making inside of the working electrode negative. Therefore, ions are repelled by the like charge in the electrode. This situation is called thermodynamic equilibrium and

preserved during the redox process [16]. The state of equilibrium is explained with Nernst Equation:

$$E = E^{o} + \frac{2.3RT}{nF}\log\frac{C_O(0,t)}{C_R(0,t)} \quad \text{.....(4),}$$

where E is the applied voltage (between working electrode and reference electrode), E^o the standard electrode potential, n the number of electrons, F the Faraday constant, R the reaction rate, and $C_O(0,t)$ and $C_R(0,t)$ the concentrations on the electroactive species in oxidation and reduction reactions, respectively [3].

So as the potential is swept from $E_{initial}$ to E_{final} (forward scan), a diffusion layer occurs and current starts flowing. After the current reaches a peak value, the equilibrium converges to full conversion of the reactant at the surface of the working electrode. Getting closer to E_{final}, current decreases until a very low value for the reason that the diffusion layer becomes vast and the flux of the reactant to the surface is not big enough to satisfy Nernst Equation [17].

1.5 Objectives of the Research

The goal of this study is based on the cyclic voltammetric (CV) analysis of dopamine in phosphate buffered saline (PBS) using vertical-aligned carbon nanotubes which are grown in hot filament chemical vapor deposition machine (HFCVD). Prominent research goals include:

- Growth of CNTs using Co catalysts on a Si substrate.
- Characterization of the material property of CNTs
- Implementation of CNTs as biosensor electrode for CV in a glass cell
- Analysis of sensed signals of DA according to varying concentrations and potential scan rates
- Comparison of CNTs' and graphite's DA sensing capability

1.6 Organization of the Thesis

- Chapter 1 presents brief introductions to electrochemical biosensor, carbon nanotubes and graphite materials and their electronic properties, nanotechnology approaches for biosensors and the use of cyclic voltammetry method for electrochemical sensor characterization.
- Chapter 2 gives an elaborated information on the growth and characterization of CNTs
- Chapter 3 reports the use of CNTs and graphite on DA sensing experiments
- Chapter 4 gives an overview and conclusion of the research and experiments described in Chapters 2 and 3
- Chapter 5 presents information about future work related to this study.

CHAPTER II

GROWTH AND CHARACTERIZATION OF CNTs

In this chapter, techniques used for carbon nanotube fabrication and characterization are explained in detail. The necessary techniques utilized are intended to give multi-walled nanotubes, which are previously described as having a conductive property. The important parameters in the vast majority of nanotubes' variation are their diameter, length, and alignment depending on their synthesis methods.

In making of CNTs, scientists had accepted catalysts [18], chemical gases [19], substrates [20], and temperature [21] as key factors. After analyzing previous studies about these factors, silicon (Si) and CH_4-H_2 gas mixture were used as substrate and gas for the CNT growth, respectively. The technique used is Chemical Vapor Deposition (CVD). According to Wong et al., temperature affects the growth rate of CNTs [22]. Besides, gas flow rate, pretreatment time, and metallic buffer layer thickness influences the alignment of CNTs and their structure.

In the experiments, hot-filament CVD system was used to grow CNTs. The system also includes a substrate heater to provide the required temperature to the substrate for better control of CNTs synthesis. Si substrate used is selected as N^+ type and its surface was etched using buffered oxide etch (BOE) before deposition of buffer and catalyst layers on the substrate. BOE cleans any native oxide on the Si substrate. The use

of N^+ type Si substrate is to provide better conductivity, thus smaller substrate resistance. The cleaned Si surface was first coated with titanium (Ti) as a buffer layer followed by cobalt (Co) as the catalyst material for CNTs synthesis. The buffer (Ti) and catalyst (Co) thicknesses obtained are 15nm and 5nm, respectively. The Ti buffer layer hinders direct interaction of Co and Si that poison the catalytic activity of Co during CNTs synthesis at high temperature.

To synthesize CNT arrays on the Si substrate, hot filament chemical vapor deposition machine (HFCVD) was employed. Methane (CH_4) gas was chosen as the carbon source for the CNT growth. Before introduction of methane, the substrate was pretreated with NH_3 gas which helps i) to remove any oxide formation on the Co catalyst due to non-ideal fabrication conditions such as Co exposure to air during substrate transferring between fabrication systems, and ii) conditioning of the Co catalyst layer into smaller particles, thereby favorite CNT growth [13]. In the experiments, an optimum pretreatment time of 40 min at NH_3 flow rate of 100 sccm was used in the pretreatment step. After the pretreatment, CH_4 was turned on in the HFCVD machine to grow CNTs on the Si substrate. This process was applied for 4 minutes. During the nanotube growth process, carbon containing specie reacts with the catalyst at high temperatures. In addition, hydrogen gas was used to keep the chamber temperature stable during growth process.

After growing CNTs, their tube diameter, vertical alignment and length were examined utilizing a scanning electron microscope (SEM), branded Hitachi 4200. In

Figure 2.1, SEM picture of CNTs grown after 4 min CH_4 flow in HFCVD machine is shown. The length of nanotubes is nearly 19µm. Besides, it is clear that their alignment is vertical.

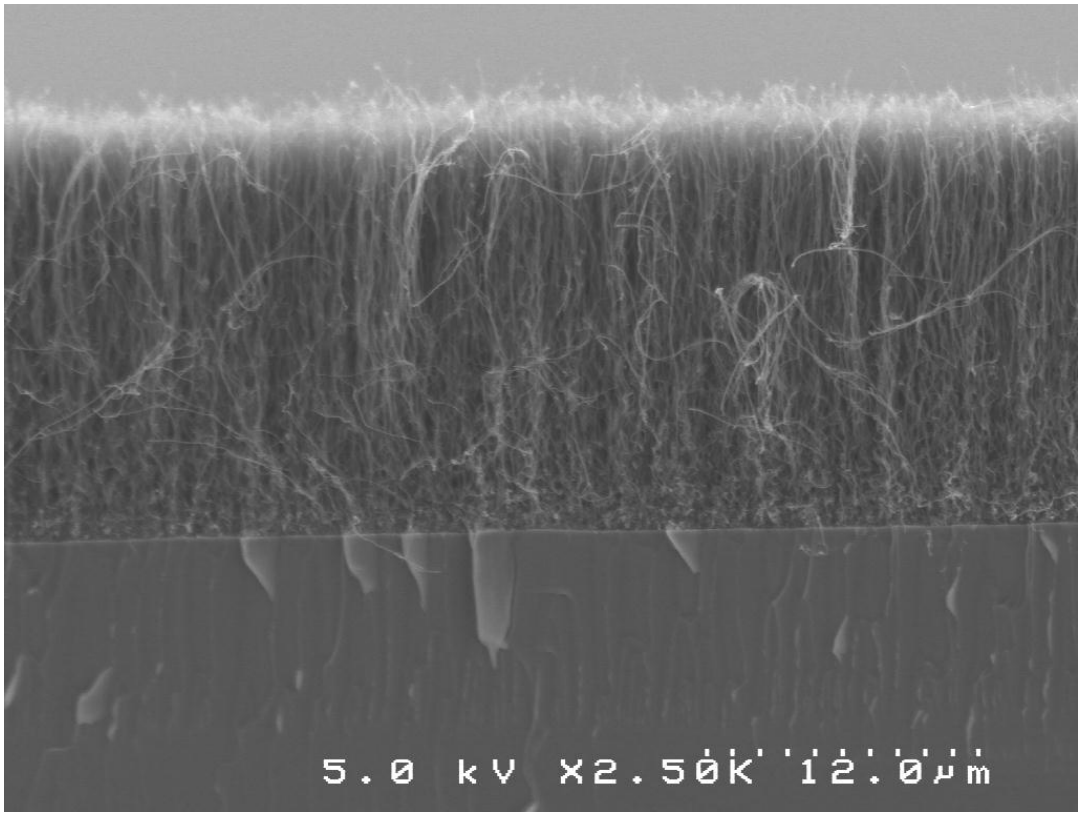

Figure 2.1: SEM picture of CNTs on N^+ type Si wafer. 4 minute flow of methane (CH_4) yielded nearly 19µm long nanotubes.

2.1 Raman Spectra of CNTs

Raman spectra of CNTs is used to identify nanotubes. In this way, one can understand whether carbon nanotubes are single walled or multi-walled, and their diameters and quality. In general, three prominent features of Raman spectra were

utilized: Radial breathing Mode (RBM), the G-band, and the D-band. All these features are created by formations of (n,m).

In RBM, carbon atoms move along the radial direction. Therefore, it is used to estimate nanotubes' diameters. The G-band refers to the vibrations in sp^2 carbons and indicates if the nanotube is metallic or semiconducting. Besides, the D-band is attributed to the dispersive disorder of nanotube formation, which yields clues about the impurities and asymmetry of CNTs [23].

In the analysis of Raman spectra of CNTs, Wong's previous studies have been referred. In his studies, Wong fabricated CNTs in our laboratories using microwave plasma CVD (MPCVD) and thermal CVD machines [24]. In Figure 2.2, typical Raman spectra of CNTs grown in our labs are shown. The spectra of thermal CVD grown CNTs demonstrates two intensity peaks: one at the raman shift of 1322 cm^{-1}, and the other one at 1591 cm^{-1}. The first and second peaks are associated with the D-band and G-band, respectively.

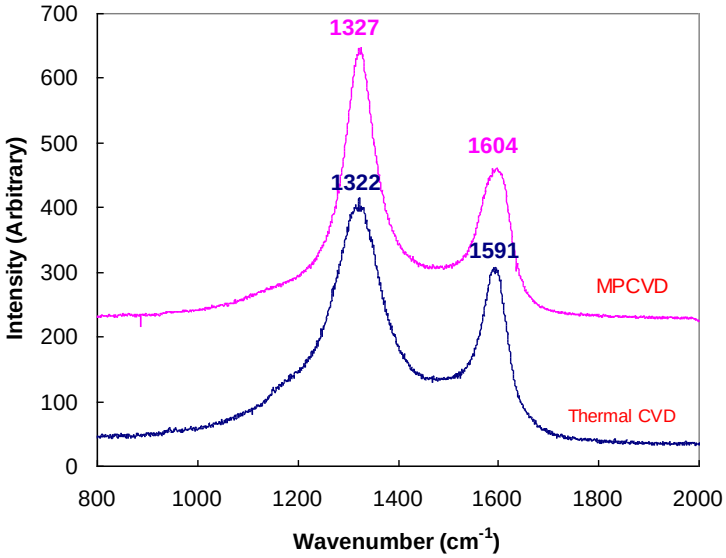

Figure 2.2: Raman spectra (Intensity vs. Wavenumber/Raman shift) of the MPCVD and thermal CVD grown CNTs [24].

It is clear from the figure that D-band's signal intensity, I(D) is higher than I(G), G-band's signal intensity. In addition, I(D)/I(G) ratio higher than 1 indicates considerable amount of impurities/defects in nanotubes. In Figure 2.2, this ratio exceeds 1, showing significant defects on CNTs. However, this is indicative of the potentially very high biosensing capability of CNTs, especially if growth with little defects.

CHAPTER III

IMPLEMENTATION OF CNT AND GRAPHITE FOR ELECTROCHEMICAL BIOSENSING OF DOPAMINE

In the following sets of experiments, dopamine was attempted to be detected in a biosensor setup. The setup consists of a reference electrode and a counter electrode which are hang vertically in a glass cell, and a working electrode laying underneath solution, and between folds of glass cell. The counter electrode is the wire made of platinum, which is a noble metal resistive to corrosion and oxidation. It is used to provide a potential difference through the working electrode. The reference electrode is a wire made of Ag/Agcl. It consists of a thin glass tube filled with 1M KCL and an AgCl coated Ag wire inside the tube. The bottom of the glass tube is porous, each pore having microns of diameters. The reference electrode is used for the measurement of the potential during a CV scan. It has very big impedance, therefore not drawing any considerable amount of current from the electrical connection of the working and counter electrodes.

The working electrodes used in the experiments are graphite and carbon nanotubes, separately. In the setup, counter and reference electrodes are hang vertically and separated from each other. They are immersed into the solvent and are placed (~4mm above) close to the working electrode to reduce resistance, which can

yield a small decrease in the current (Fig. 3.1). The working electrode is placed on the copper line, and a plastic o-ring is put on top of it. The plastic ring enables the working electrode to get in touch with the electrolyte, while preventing the electrolyte from leaking outside the functional part of the working electrode. The effective sensing area of the working electrode is therefore defined by the o-ring opening.

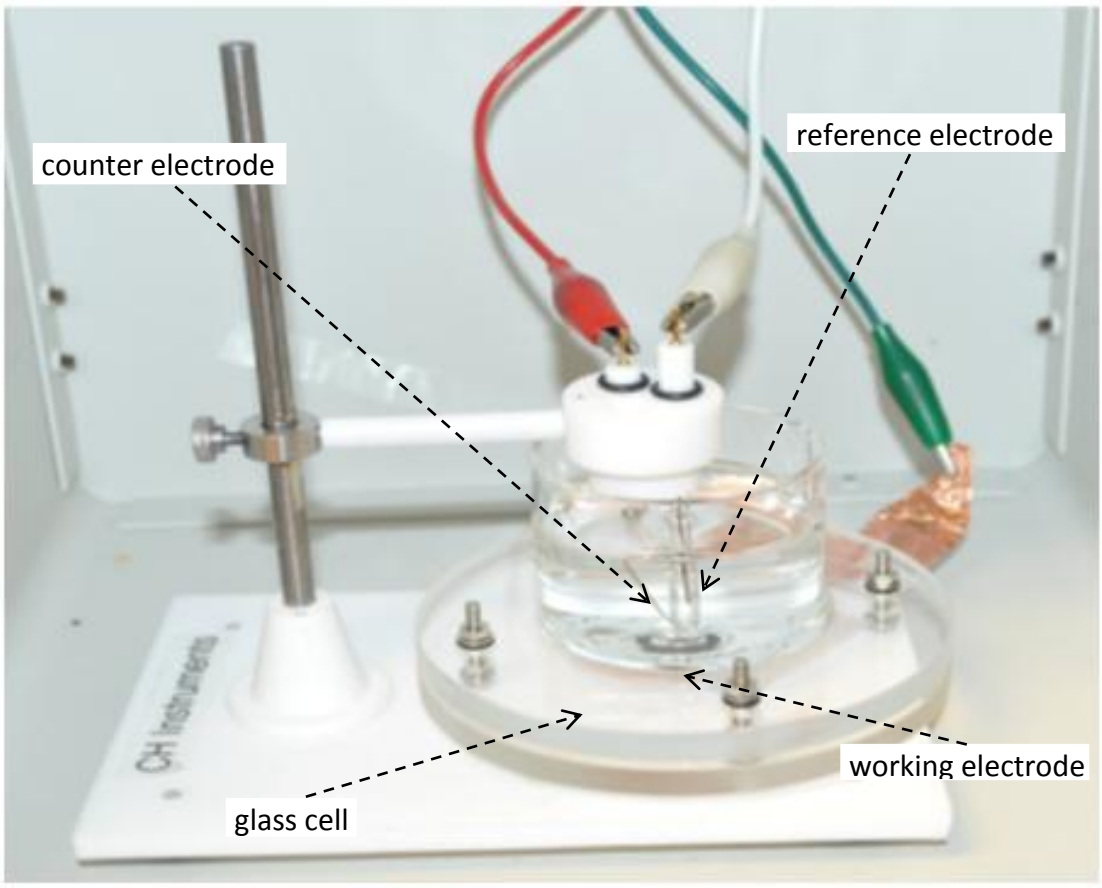

Figure 3.1: Biosensing setup with three electrodes inside a glass cell. The electrodes are connected to faraday cage and a current amplifier system through wires.

During the biosensing experiments, the glass cell was put into Chi Faraday Cage to keep any electromagnetic distortion away from the setup. All the electrodes were

then connected to CHI-200 Picoamp booster, which amplifies very small currents flowing through the working electrode. Following that, CV scan and analysis of the measurements were conducted in CHI 660 electrochemical analyzer.

Before measuring the dopamine sensitivity of the biosensor setups, the quality of the working electrodes was tested and then the electrodes were characterized. To perform the test, ferrocyanide ($Fe(CN)_6^{3-/4-}$) redox couple was used in a 0.1 M KCL solvent [25]. Ferrocyanide is a very popular compound which is used for testing the redox reaction quality of the electrodes in biosensing experiments. The reversible redox reaction involves oxidation of ferrocyanide ($Fe(CN)_6^{4-}$) to ferricyanide ($Fe(CN)_6^{3-}$) and reduction of the latter to the first one. Since the ferrocyanide couple includes single electron transfer and no chemical reactions, it shows a nearly ideal quasireversible characteristic. Furthermore, ferrocyanide redox couple is very appropriate for testing carbon electrode since the ions of the solution sticks trivially to carbon [26]. Besides, 0.1 Mole (M) potassium chloride (KCL) is used as the electrolyte, which is utilized as an electrically conducting solution.

In the experiments, scan rates of 10, 50, 100, 200 and 500mV/s were used. Initial step of all the biosensing experiments include running cyclic voltammetry only with the electrolyte itself. The recorded signal is called the background signal. Then, reactant solution is added into the electrolyte and the CV analysis aimed at examining the electrode sensitivity for the target specie is performed. The resulting curve contains data regarding the electrolyte and the reactants. Hence, background curve is subtracted

from that hybrid curve and a simple curve concerning only the target species' CV analysis on the specific working electrode is obtained.

First bunch of experiments was conducted using graphite working electrode at 5 different scan rates (10, 50, 100, 200, and 500mV/s). In addition, 5 different ferrocyanide concentrations (1, 2, 3, 4, and 5mM) were tested. However, only 10, 50, 200, and 500mV/s scan rates were used for 5mM ferrocyanide, where 100mV/s was applied to all 5 concentrations. The potential window used is between -0.5V and +1V. In Figure 3.2, 5 concentrations of ferrocyanide were swept at 100mV/s and the resulting curves were overlaid on top of each other. From the figure, it is observable that Equation 3 is accommodated. It is also clear that the redox current peaks are observed and the peak height increases with higher concentrations of ferrocyanide. The CV curves are also reversible for all concentrations. 5mM ferrocyanide gives the highest current peak amplitude (~0.2mA), which is remarkable.

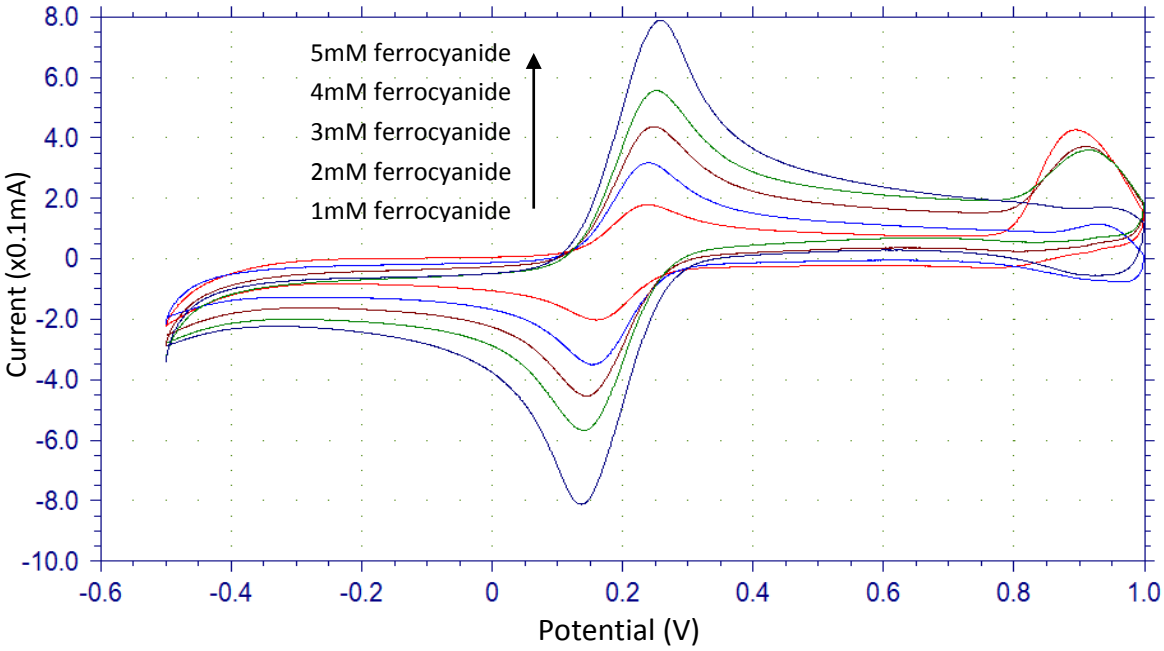

Figure 3.2: Voltage sweep curves of 1, 2, 3, 4, and 5mM $Fe(CN)_6^{4-}$ on graphite electrode at 100mV/s.

Moreover, concentration of the reactant increases the current peak proportionally, as shown in Figure 3.3. The curves for oxidation and reduction indicate a linear correlation between the current and concentration. Thus, graphite is proven to be capable for further biosensing experiments.

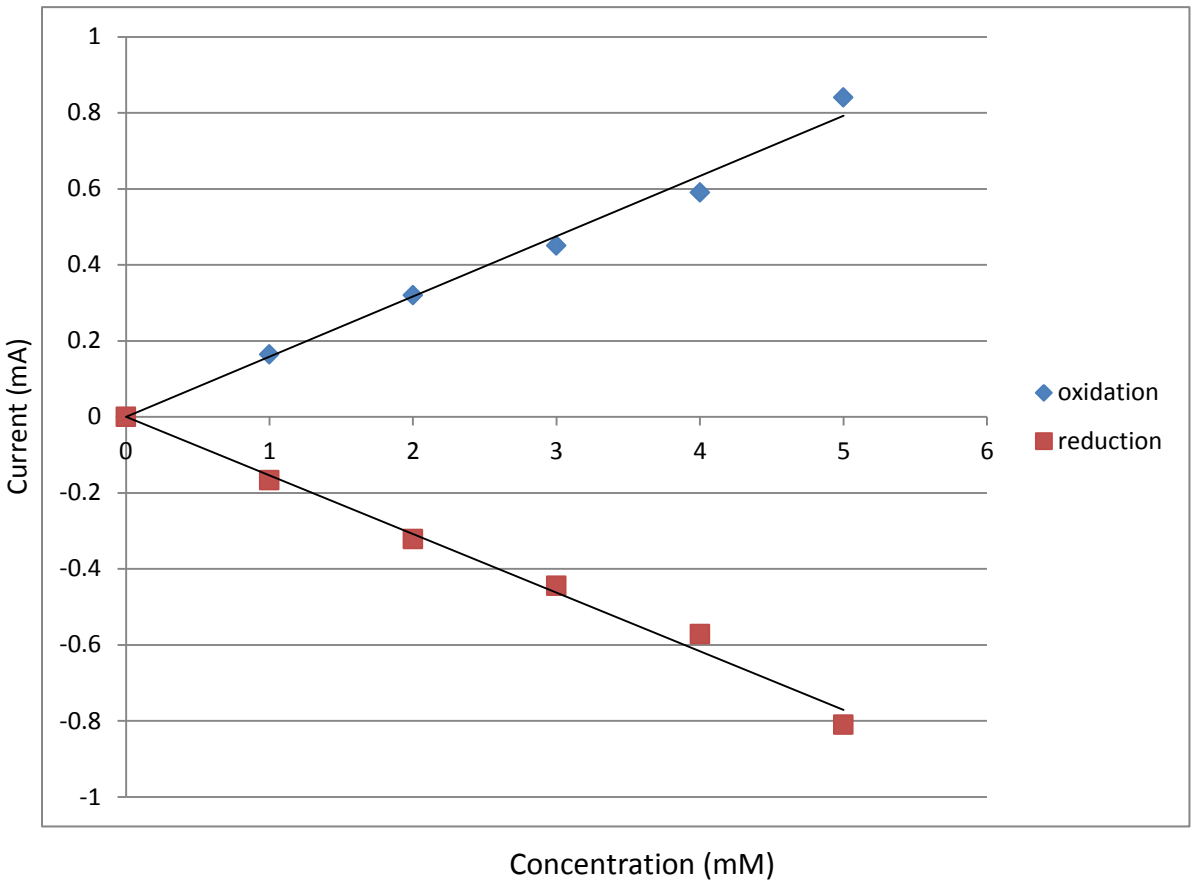

Figure 3.3: Concentration versus current curves for the redox reactions obtained after the CV scan of ferrocyanide on graphite electrode at 100mV/s.

In Figure 3.4, CV sweep curves of all the scan rates for 5mM $Fe(CN)_6^{3-/4-}$ were plotted. Since increasing $\sqrt{\nu}$ (where ν is the scan rate (SR)) increases the peak current according to Cottrell Equation (3), the values of these two parameters are proportional to each other.

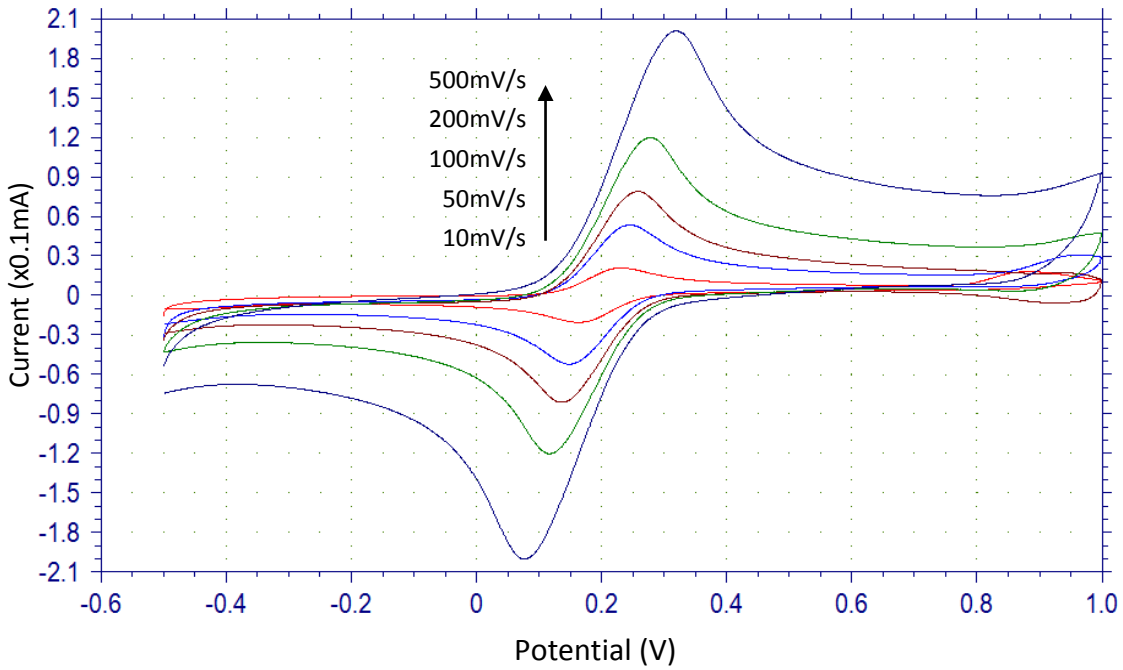

Figure 3.4: 5mM Ferrocyanide CV scans with the scan rates of 10, 50, 100, 200, and 500mv/s (from red to navy blue) where KCL background CV curves for the respective scan rates are subtracted.

After obtaining gradual increase in the I-V curves of the CV scan with respect to enhancing scan rates, Figure 3.5 was obtained. It concurs to the Cottrell Equation, showing the linear increase in the cathodic and anodic peak currents with the increase in the square root of the scan rate.

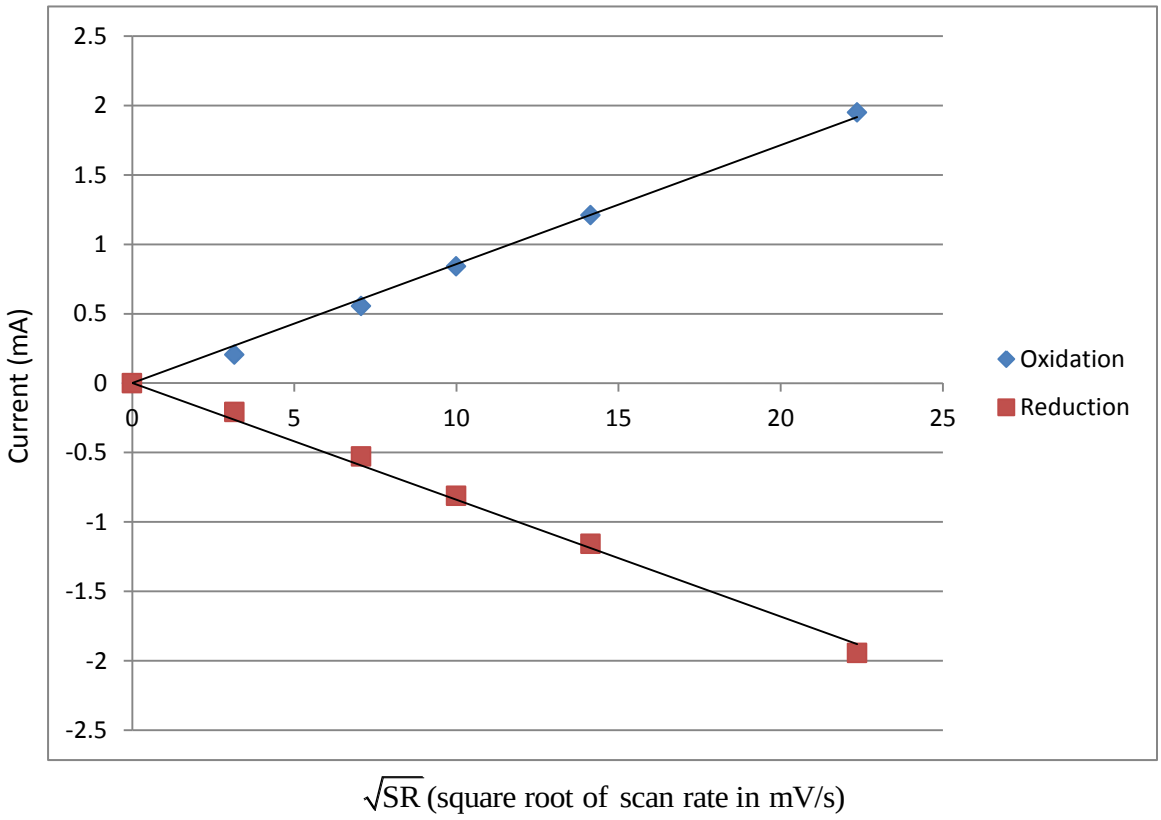

Figure 3.5: $\sqrt{SR}$ versus redox peak current of 5mM ferrocyanide on graphite electrode where SR refers to scan rate (10, 50, 100, 200, and 500mV/s).

Afterwards, Ferrocyanide sensing was performed using a CNT working electrode. Figure 3.6 (a) and (b) show the corresponding CV and calibration curves in various ferrocyanide concentrations, respectively. In Figure 3.6 the concentration linearly increases the peak current of the redox reactions. The highest oxidation peak current is 0.5 mA, which is higher than [27] at higher ferrocyanide concentrations. In addition, the effect of scan rate on the peak current (Fig. 3.7) is again proved as expected for multi-walled CNT electrode.

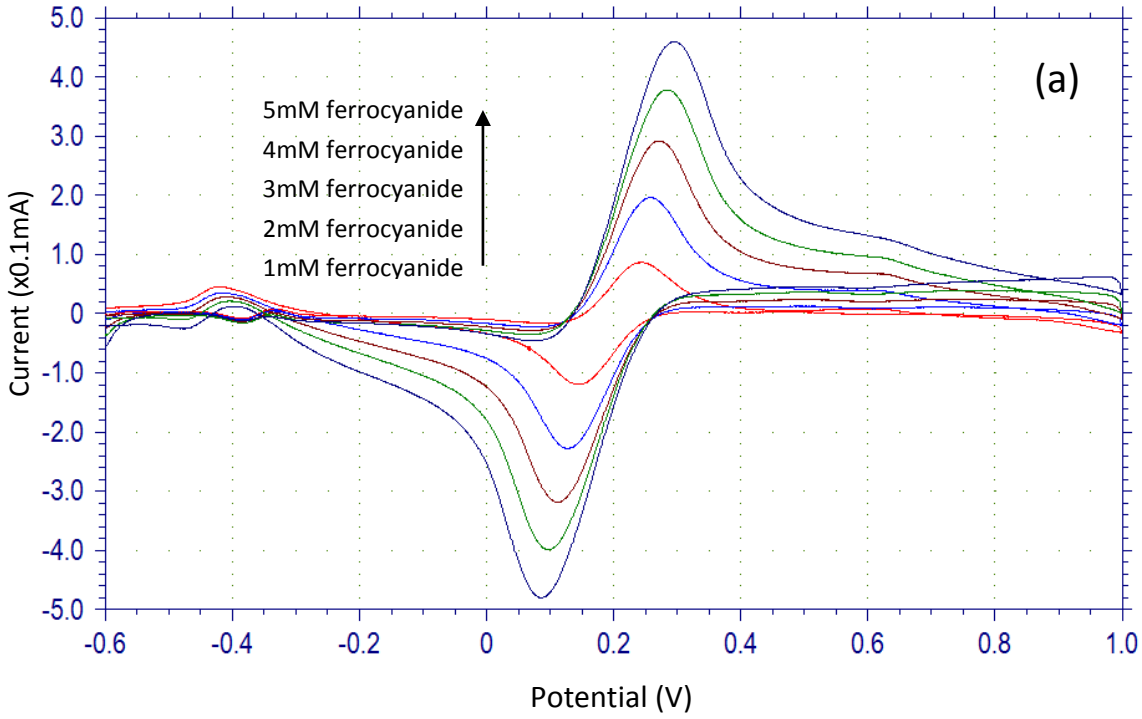
(a)
5mM ferrocyanide
4mM ferrocyanide
3mM ferrocyanide
2mM ferrocyanide
1mM ferrocyanide
Current (x0.1mA)
Potential (V)
5.0
4.0
3.0
2.0
1.0
0
-1.0
-2.0
-3.0
-4.0
-5.0
-0.6
-0.4
-0.2
0
0.2
0.4
0.6
0.8
1.0

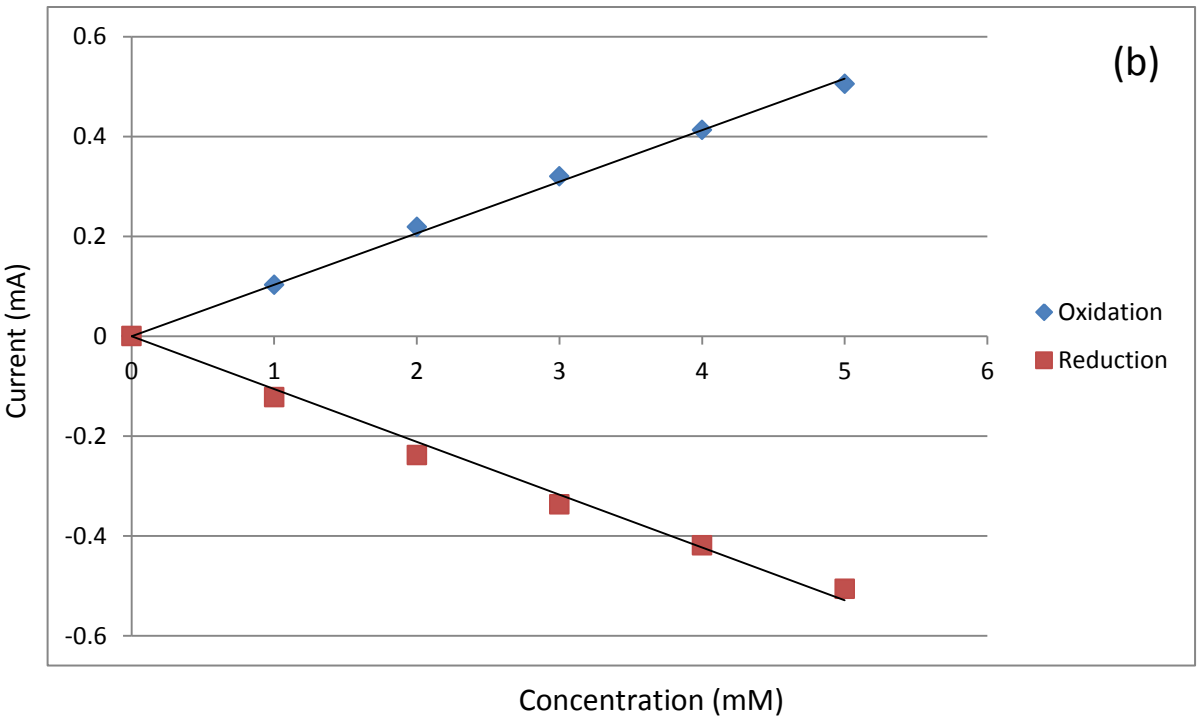

Figure 3.6: Concentration (1-5mM) versus current curves for the ferrocyanide redox reactions on CNT electrode, operating at a constant scan rate of 100mV/s. (a) CV curves, and (b) calibration curves.

Before performing ferrocyanide experiment on graphite electrode, the optimum potential window was determined by using a big window (-2V to +1.5V) at slow scan rate (10mV/s). From this experiment, a lower potential window, which ranges from -0.5V to +1V was selected. Shrinking the potential window facilitated the progress of the experiment. In this way, the potential sweep time was reduced and the solution was protected from further oxidation. However, the use of bigger window beforehand had already changed the surface of the graphite electrode. Its surface blistered with the exposition to high potential for a long time (caused by the slow scan rate). Hence, the graphite electrode had bigger surface to volume ratio than its normal condition. As a result, higher surface area allowed graphite electrode with more electrons and thus,

draw higher redox currents. This behavior is verified in Figures 3.3 and 3.5 for comparative concentrations and voltage scan rates in Figures 3.6 and 3.7, respectively. Therefore, altered surface of graphite can yield higher currents than CNT in CV experiments.

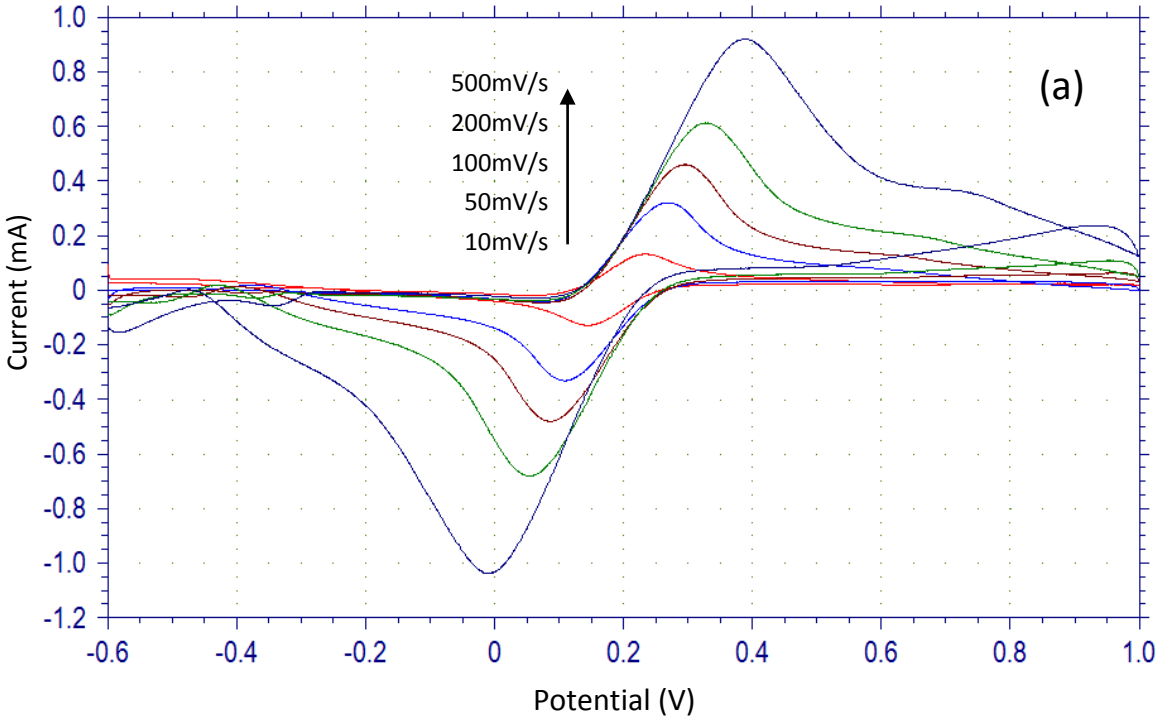

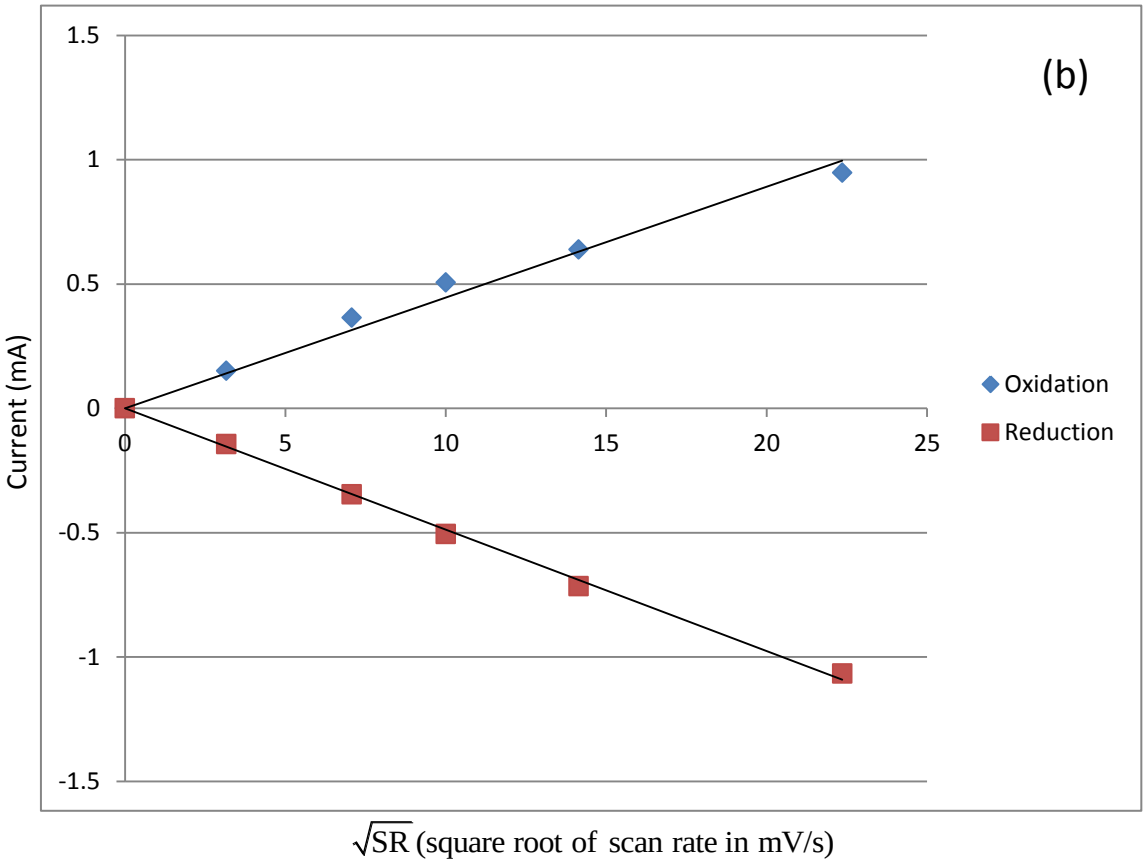

Figure 3.7: $\sqrt{SR}$ versus redox peak current of 5mM ferrocyanide on CNT electrode where SR refers to scan rate (10, 50, 100, 200, and 500mV/s). (a) CV curves, and (b) calibration curves.

After verifying the feasibility of graphite and CNT electrodes for electrochemical biosensing experiments, dopamine neurotransmitter was used as target specie for the pursuing biosensing experiments. In these experiments, phosphate buffered saline (PBS) was used as an electrically conductive electrolyte. The PBS concentration was selected as 0.1M and the same bunch of voltage sweep rates was employed. However, voltage window was altered to a different one as -0.5V to +0.8V, which is almost same as the first one.

The first group of DA sensing experiments was conducted on graphite working electrode. Utilizing a smaller potential range did not change the surface of the graphite significantly. Therefore, a better comparison of graphite and carbon nanotube electrodes can be done in DA sensing.

Unlike ferrocyanide in KCL, four different peaks were observed after every cyclic voltammetric experiment which was targeted at sensing dopamine in PBS (Fig. 3.8). The reason for this behavior is based on the reactions taking place in the CV scan. The reactions involved are called ECE reactions [28]. ECE reaction mechanism consists of electrochemical, chemical, and electrochemical reactions again, in order. Two electrochemical reactions, which are presented in the experiments and also relevant to ECE mechanism, are as follow:

$$\text{dopamine} \rightleftharpoons \text{o-quinone} + 2H^+ + 2e^- \qquad 3.1,$$

and

$$\text{leucodopaminechrome} \rightleftharpoons \text{dopaminechrome} + 2H^+ + 2e^- \qquad 3.2.$$

On the other hand, the chemical reaction involves cyclization of o-quinone to indole. Following that, indole oxidizes into leucodopaminechrome [28]. Therefore, this chemical reaction breaks the thermodynamic equilibrium of the system.

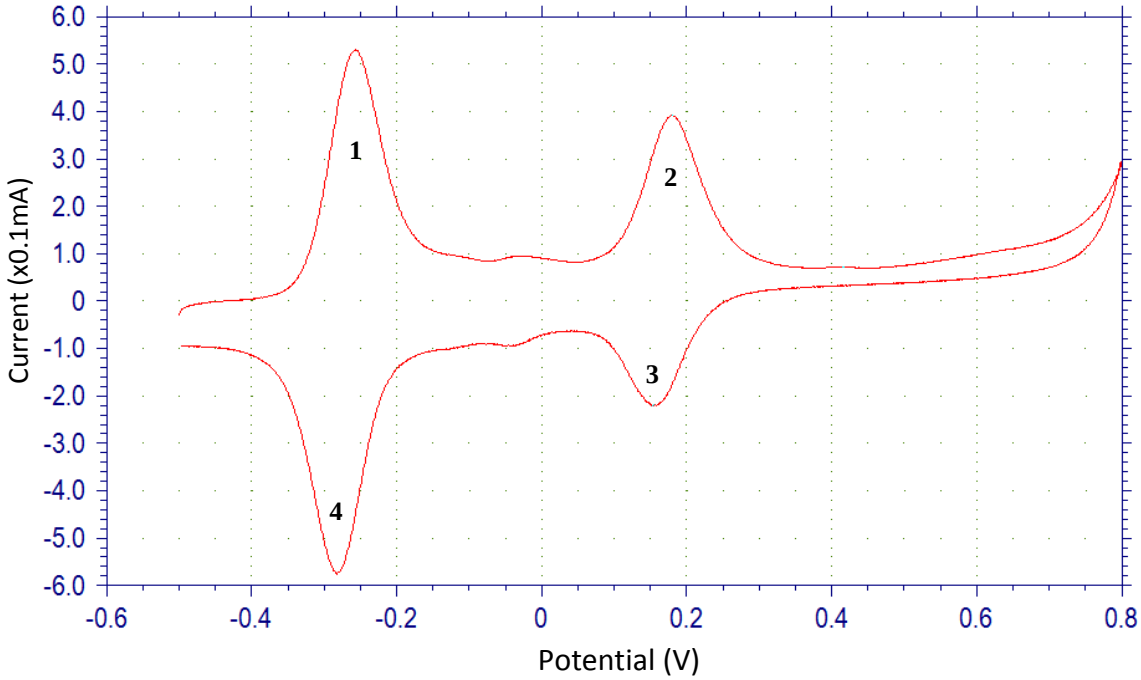

Figure 3.8: Voltage sweep curve of 400µM dopamine on graphite at 100mV/s. Four separate redox peaks (labeled with numbers 1-4) can be seen.

In Figure 3.8, four oxidation/reduction peaks correspond to the following reactions are observed:

1: leucodopaminechrome → dopaminechrome + $2H^+$ + $2e^-$

2: dopamine → o-quinone + $2H^+$ + $2e^-$

3: o-quinone + $2H^+$ + $2e^-$ → dopamine

4: dopaminechrome + $2H^+$ + $2e^-$ → leucodopaminechrome

Thus, dopamine neurotransmitter engaged reactions are related to second peak of oxidation and the first peak of reduction. In the forward CV scan's (-0.5V to +0.8V)

second peak, dopamine diffuses onto the working electrode and releases electrons, which are caught by the working electrode. Then, o-quinone is released outward of working electrode. In the reverse scan (+0.8V to -0.5V), o-quinone is reduced to dopamine. Throughout this process, o-quinone diffuses onto the working electrode and captures electrons from the working electrode. This results as the flow of anodic current through the working electrode.

In DA sensing experiments, 5 different DA concentrations (100, 200, 400, 600, and 800µM) were scanned in 0.1M PBS solution (Fig. 3.9). The CV scans gave gradually increasing redox current peaks with the increasing DA concentrations.

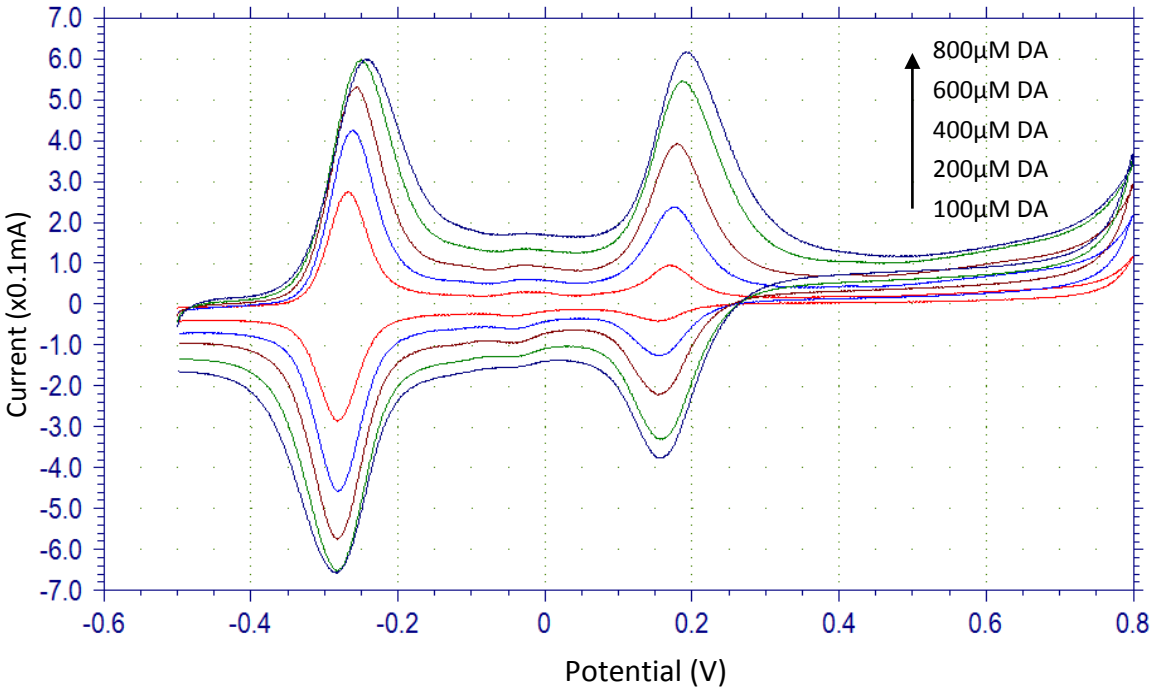

Figure 3.9: Voltage sweep curves of 100, 200, 400, 600, and 800µM dopamine on graphite at 100mV/s.

This two-sided increase is verifiable by Cottrell Equation (3) according to Figure 3.10. That is, the straight lines' correlation coefficients are very close to 1.

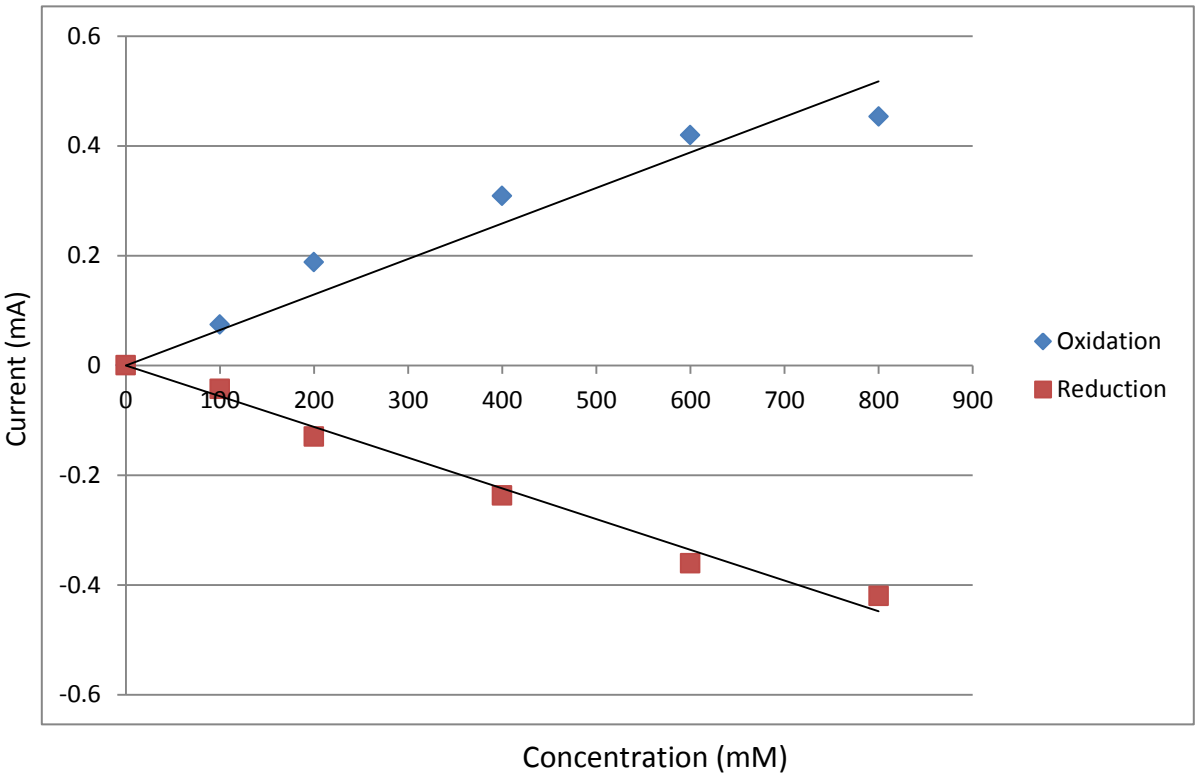

Figure 3.10: Concentration (100, 200, 400, 600, and 800µM) versus current curves for the redox reactions obtained after the CV scan of dopamine with graphite electrode at 100mV/s.

In case of analyzing the effect of square root of scan rate on the redox current peaks, 200µM of dopamine was selected. The scan rates employed were same as the first bunch of experiments: 10, 50, 100, 200, and 500mV/s. Referring to Figure 3.11, graphite is counted as an efficient working electrode. The lowest oxidation peak current involving dopamine at 10mV/s is nearly 21µA, where the highest one at 500mV/s is 85µA. This current range for graphite is higher than the ones seen in [29].

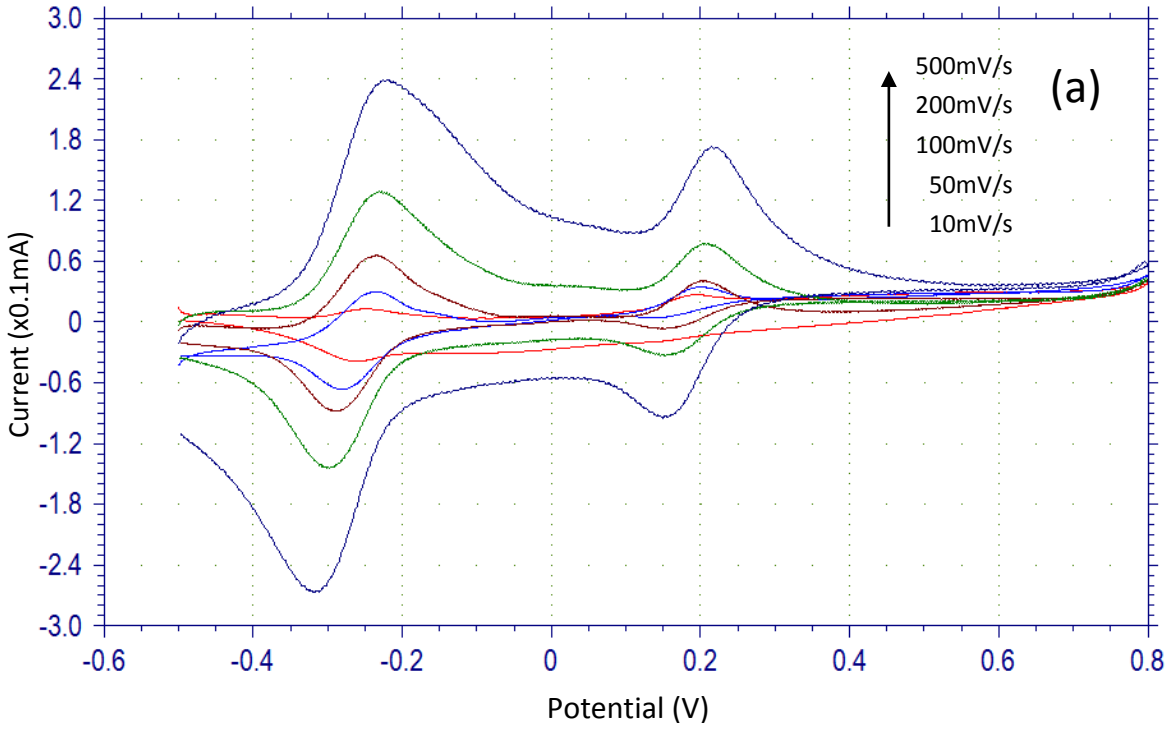
3.0
2.4
1.8
1.2
0.6
0
-0.6
-1.2
-1.8
-2.4
-3.0
Current (x0.1mA)
-0.6
-0.4
-0.2
0
0.2
0.4
0.6
0.8
Potential (V)
500mV/s
200mV/s
100mV/s
50mV/s
10mV/s
(a)

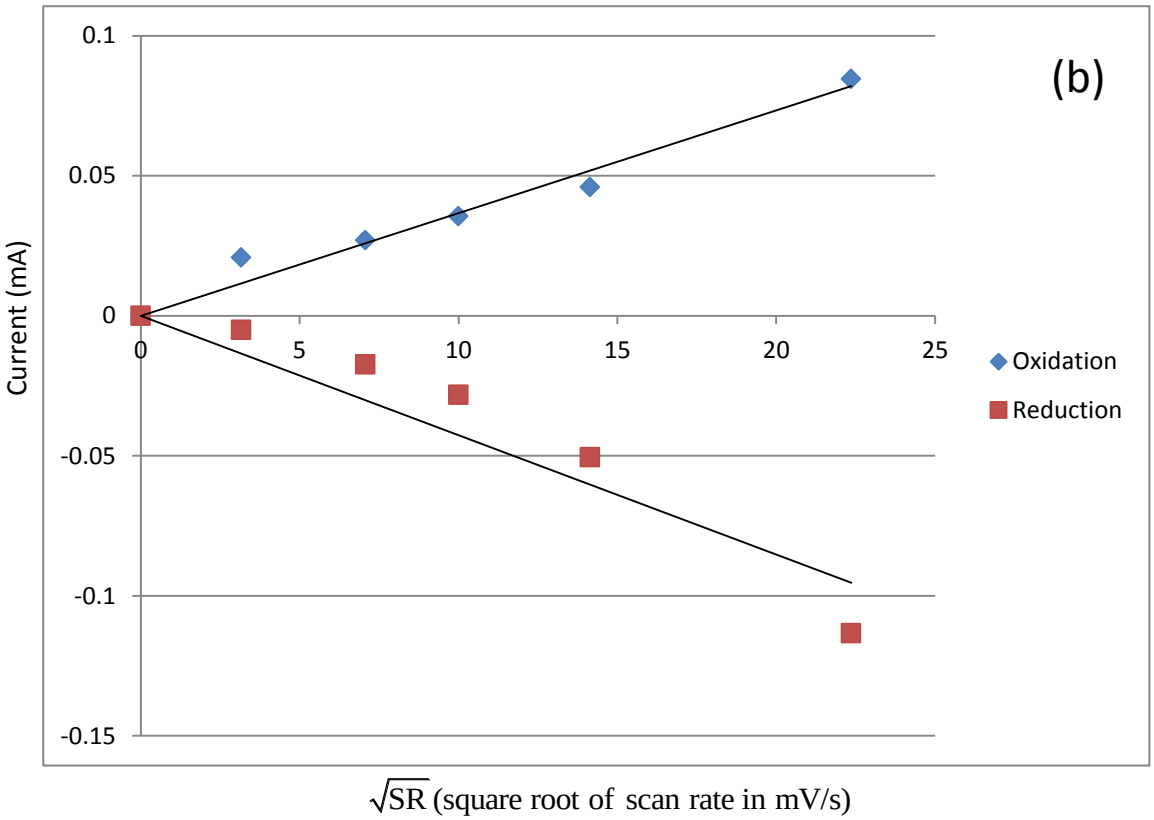

Figure 3.11: $\sqrt{SR}$ versus redox current peak height of 200µM dopamine on graphite electrode where SR refers to scan rate (10, 50, 100, 200, and 500mV/s). (a) CV curves, and (b) calibration curves.

The last group of CV experiments was conducted using multi-walled CNT electrodes for dopamine detection in 0.1M PBS solution. Firstly, 5 different concentrations of DA were exposed to CV scan at 100mV/s. Figure 3.12 (a) and (b) show the corresponding CV and calibration curves in various DA concentrations, respectively. The resulting curves showed a progressive increase in the redox peak current with respect to DA concentration.

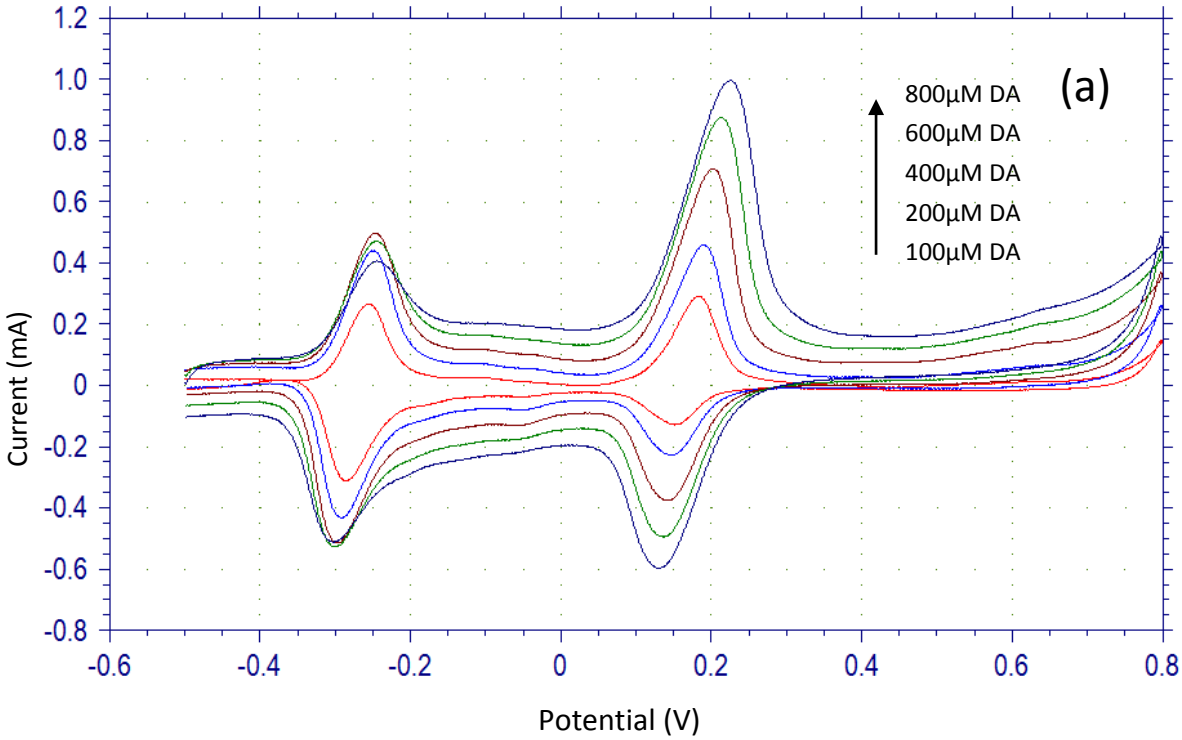
(a)
800μM DA
600μM DA
400μM DA
200μM DA
100μM DA
Current (mA)
Potential (V)
1.2
1.0
0.8
0.6
0.4
0.2
0
-0.2
-0.4
-0.6
-0.8
-0.6
-0.4
-0.2
0
0.2
0.4
0.6
0.8

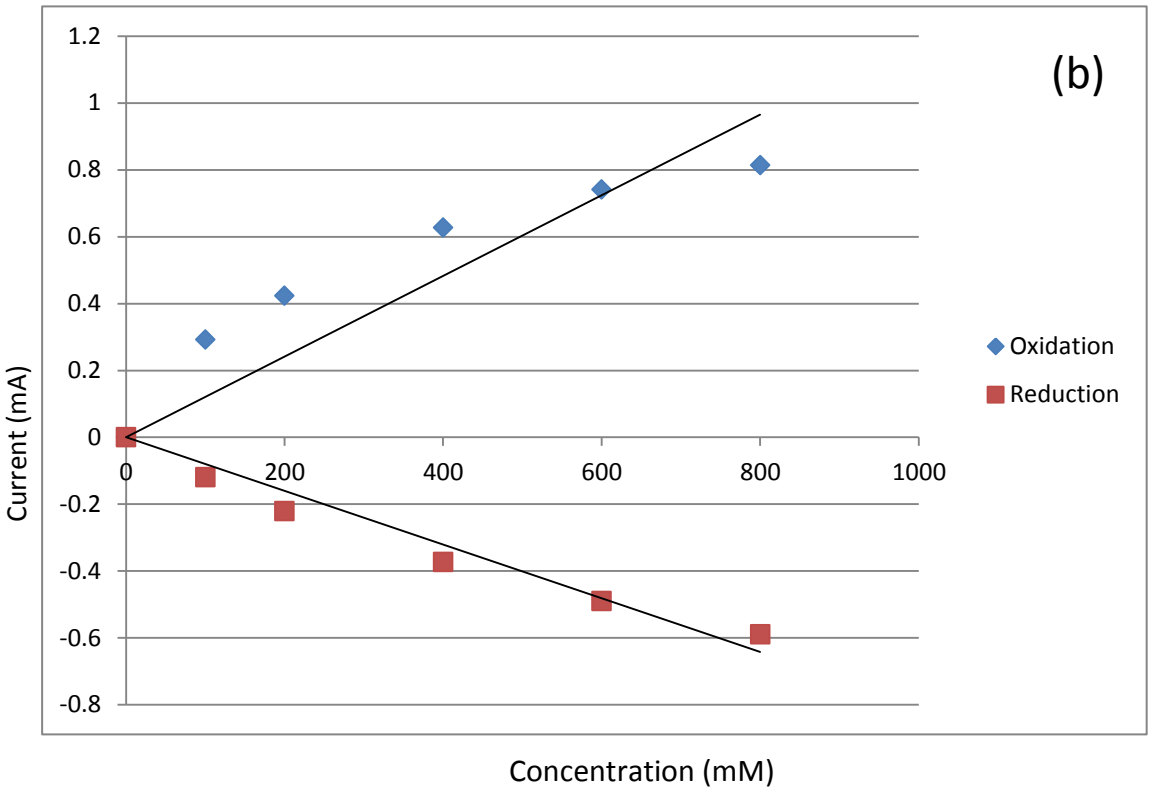

Figure 3.12: Concentration (100, 200, 400, 600, and 800µM) versus current curves for the DA redox reactions at CNT electrode, operating at a constant scan rate of 100mV/s. (a) CV curves, and (b) calibration curves.

In Figure 3.12, as the DA concentration increases, redox current peaks increase. However, this increase is slightly deviated from the linearity. The slight distorting effect needs to be further explored.

From Figure 3.13, it is clear that CNT gives higher peak currents than graphite for different concentrations of dopamine. Therefore, CNTs can be accepted as better electrodes than graphite for detection of dopamine from low to higher concentrations. The reason for this is CNTs' higher surface area, which enables more electrons to be transferred during redox reactions between dopamine and o-quinone.

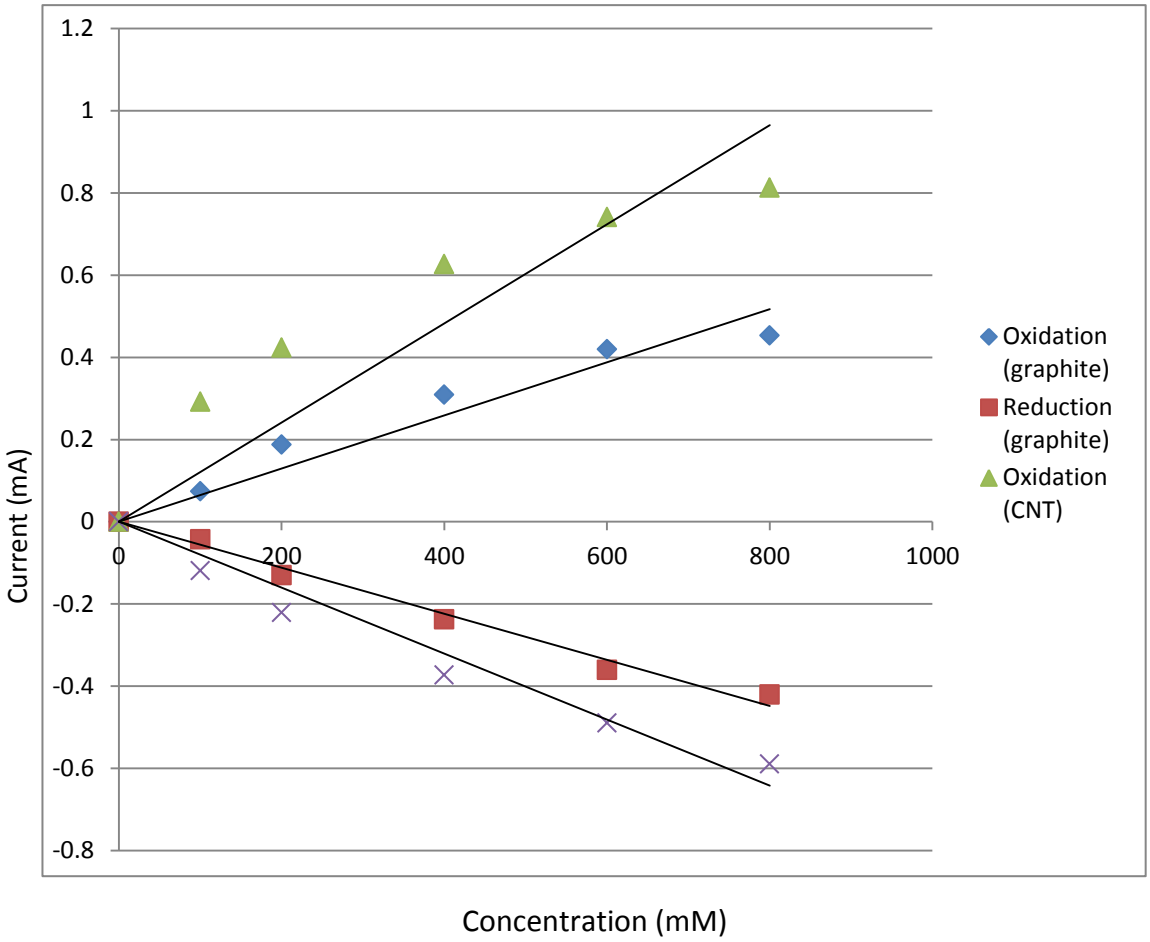

Figure 3.13: Comparison of concentration (100, 200, 400, 600, and 800µM) versus current curves for the redox reactions obtained after the CV scan of dopamine with CNT and graphite electrodes, separately at 100mV/s. Dashed and solid lines correspond to graphite and CNT working electrodes, sequentially.

Besides, the effect of the scan rate, which is another effective variable in the current peaks was analyzed with vertically aligned multi-walled CNTs taking role as working electrode. The scan rates used are same as the ones used in the experiments performed for ferrocyanide sensing. In Figure 3.14 (a) and (b), redox current peaks are remarkable ranging up to nearly 1.03mA and 1.02mA for oxidation and reduction, respectively.

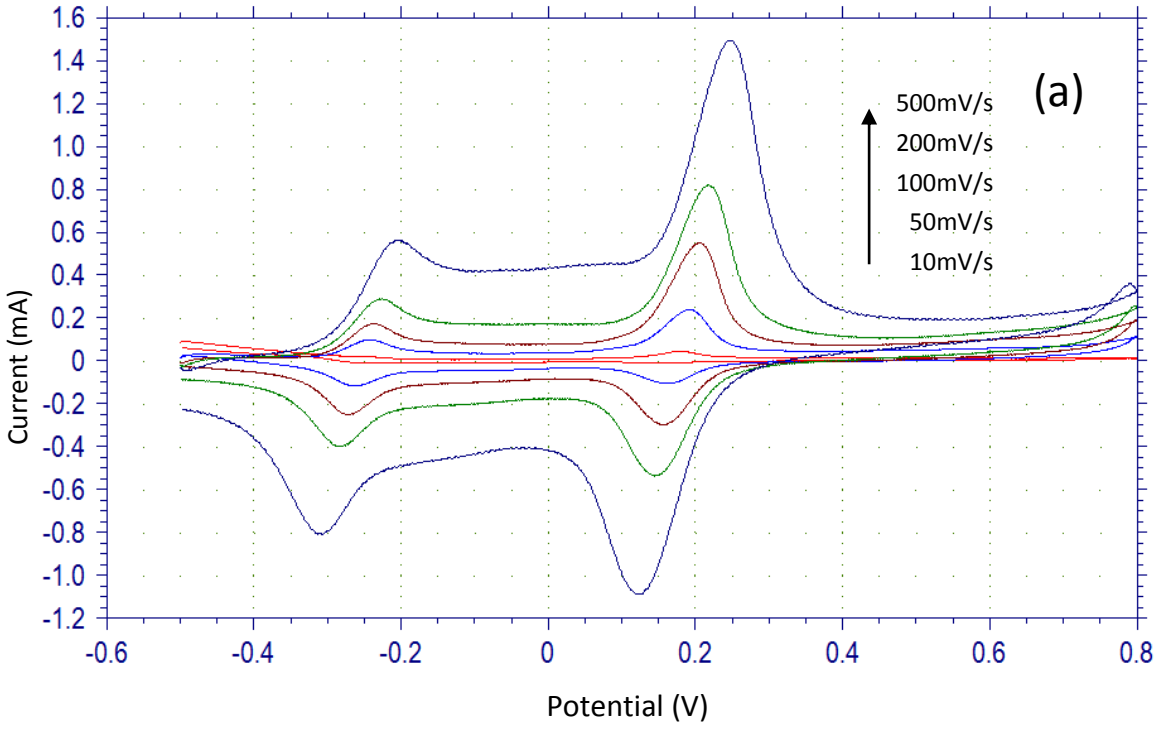
(a)
500mV/s
200mV/s
100mV/s
50mV/s
10mV/s
Current (mA)
Potential (V)
1.6
1.4
1.2
1.0
0.8
0.6
0.4
0.2
0
-0.2
-0.4
-0.6
-0.8
-1.0
-1.2
-0.6
-0.4
-0.2
0
0.2
0.4
0.6
0.8

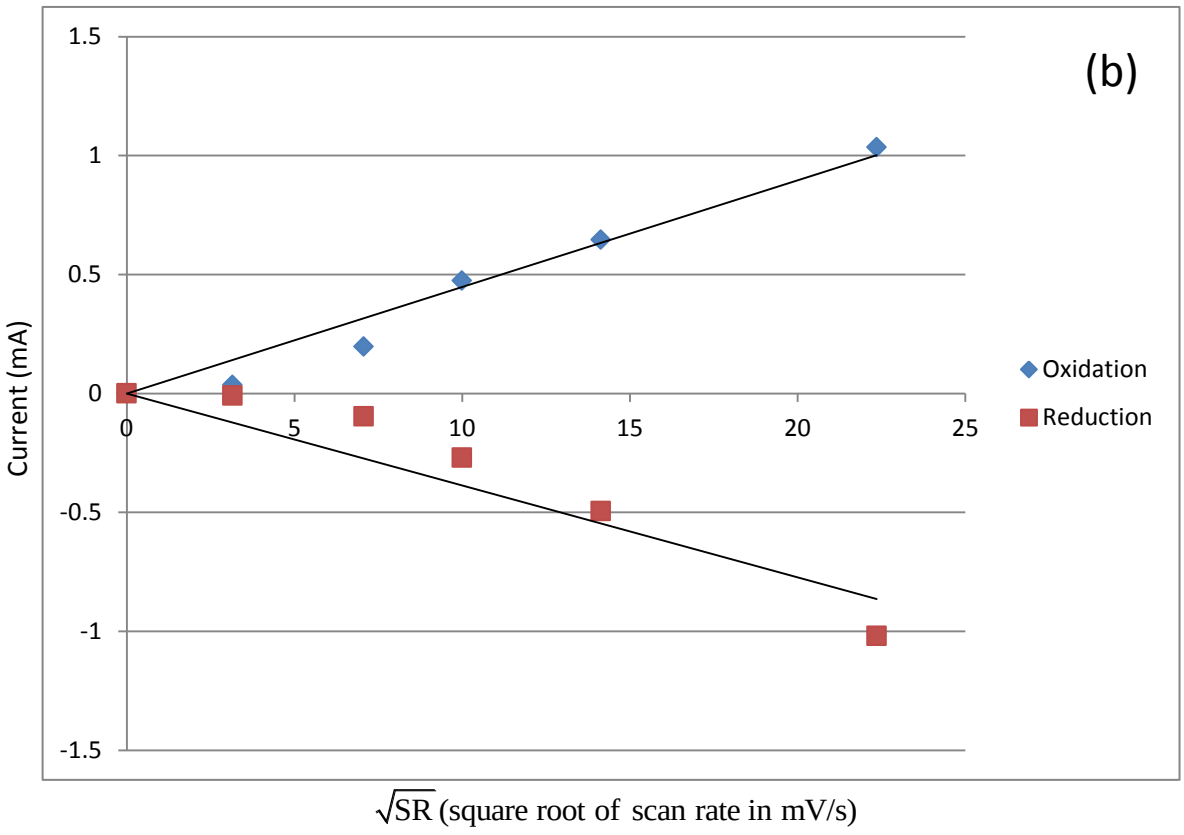

Figure 3.14: $\sqrt{SR}$ versus redox peak current of 200µM dopamine on CNT electrode where SR refers to scan rates (10, 50, 100, 200, and 500mV/s). (a) CV curves, and (b) calibration curves.

After proving nanotubes as efficient electrodes at varying scan rates in the sensing of dopamine, a comparison of them with graphite was graphed on Figure 3.15. On the figure, it is clear that CNT is a lot more efficient in progressive scan rates in detecting dopamine in electrochemical reaction than graphite

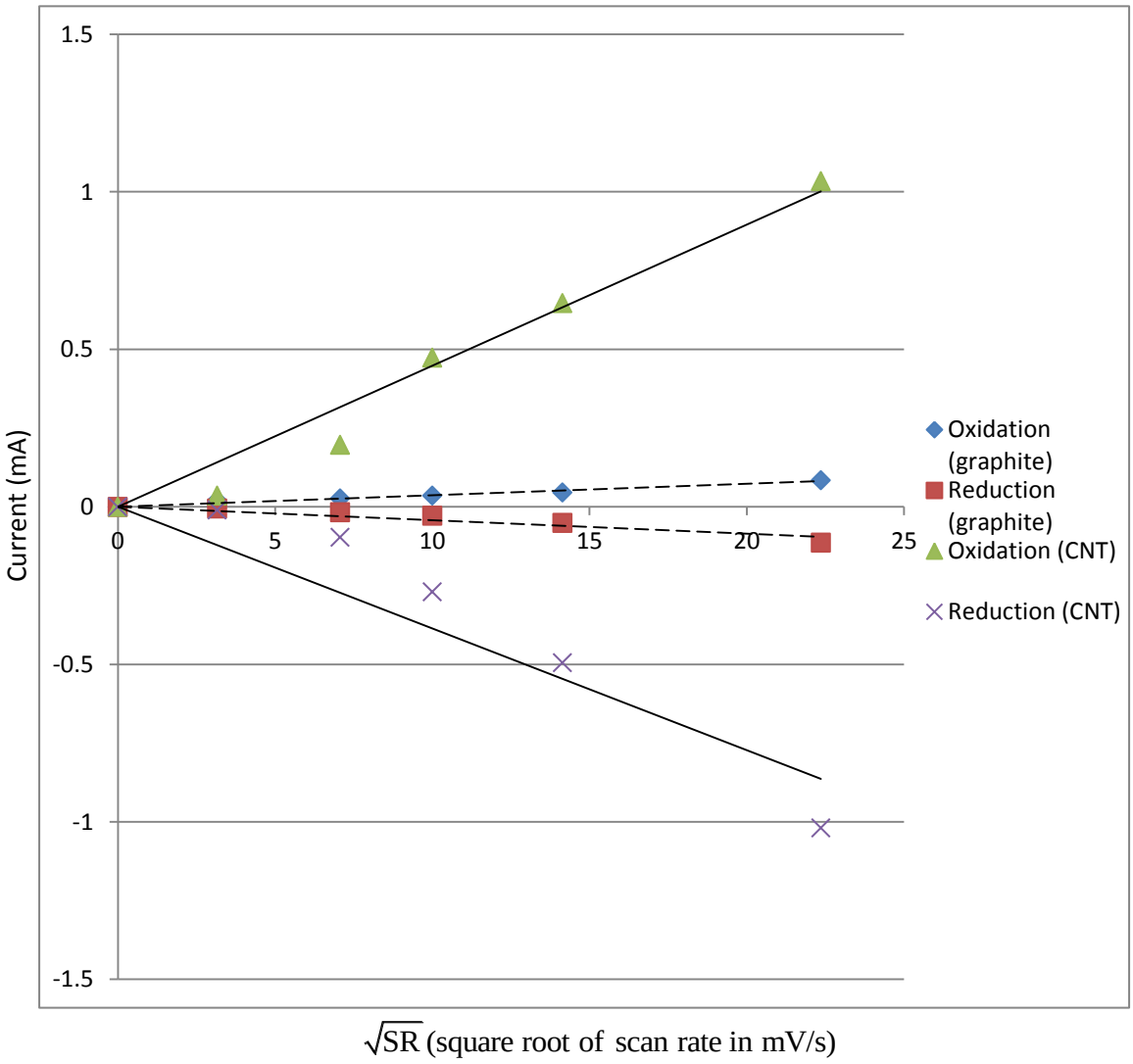

Figure 3.15: Comparison of $\sqrt{SR}$ versus redox peak current of 200µM dopamine with CNT and graphite electrodes, separately, where SR refers to scan rates (10, 50, 100, 200, and 500mV/s). Dashed and solid lines correspond to graphite and CNT working electrodes, sequentially.

CHAPTER IV

CONCLUSION

In the first experiments, multi-walled CNTs were grown on Si substrate. Multi-walled CNTs were utilized for the electrochemical biosensor experiments because of their good electrical conductivity, high surface area, and chemical stability.

Following their growth on the highly conductive N^+ type Si substrate, CNTs were first characterized by SEM and Raman spectroscopy to verify their material and electronic properties. Then, they were used as working electrodes for the biosensing experiments. In this group of experiments, sensing capabilities of graphite and CNT were observed for both ferrocyanide and dopamine.

After the CV scans of both CNTs and graphite in a KCL electrolyte solution, curves of redox peak current versus potential were seen. For both electrodes, the curves looked like rectangular with rounded edges at currents where potentials started changing from $E_{initial}$ to E_{final}, and E_{final} to $E_{initial}$, respectively. When ferrocyanide was added to 0.1M KCL solution, graphite gave higher redox current peaks than CNT due to surface blistering in high voltage (-2V to 1.5V) CV scans. The random blistering of graphite surface enhances the electrode sensitivity but reduces the cycle life. Ferrocyanide experiments also showed that graphite and CNTs both give promising cyclic voltammograms. It was found that the ferrocyanide concentration and scan rate

had directly proportional relation with the amplitude of redox current peaks abiding by the Cottrell Equation. Both electrodes gave reversible ferrocyanide redox reactions.

Dopamine sensing experiments had different behavior than ferrocyanide ones. There were four peaks observed, where only 2 of them were related with the presence of dopamine: oxidation of dopamine to o-quinone, and reduction of o-quinone to dopamine. Also observed in the CV was the redox reaction of leucodopaminechrome.

In conclusion, CNTs have provided themselves as efficient materials to be used as working electrodes in DA sensing experiments. Led by their very high surface area, CNTs are electrically better working electrodes than graphite, and give higher redox current peaks at same potentials. Compared to graphite made of superposed graphene sheets, CNTs also have a more stable structure in biosensing experiments. The bonding of nanotubes with the substrate provides stability and thus high cycle life in biosensing experiments.

CNTs have high redox current peaks for dopamine, which are better than other electrodes developed by other scientists [30, 31, 32, and 33]. This can again be attributed to the high surface area of CNTs and their very low resistance.

CHAPTER V

RECOMMENDATIONS

This study has demonstrated that graphite and CNTs are promising electrode materials for DA detection. Taking the results into consideration, many innovative ideas could be applied on the biosensing systems regarding working electrode, the most important part of a biosensing setup:

- Synthesis of CNTs on flexible conducting substrate to improve the form factor and provide better conductance of working electrode with the electrochemical analysis device's input.
- Modification of graphite's surface so that the surface becomes more stable, as well as effective.
- Conducting DA detection experiments in the presence of ascorbic acid and uric acid, which are present with dopamine in real environments.
- Modification and functionalization of CNT surface to enhance the detection of other types of biochemical.
- Design and implementation of signal processing unit to boost the biosensor's micro-scale current and transmit it to an analysis device.

REFERENCES

[1] Robert S. Marks, David C. Cullen, Isao Karube, Christopher R. Lowe, and Howard H. Weetall, “Handbook of Biosensors and Biochips”, Chapter 3, John Wiley & Sons, 2007

[2] Daniel R. Theâvenot, Klara Toth, Richard A. Durst, and George S. Wilson, “Electrochemical Biosensors: Recommended Definitions and Classification”, Pure Appl. Chem., Vol. 71, No. 12, pp. 2333-2348, 1999

[3] Joseph Wang, “Analytical Electrochemistry”, John Wiley & Sons, Inc., 2006

[4] Kim Rogers, “Principles of Affinity-based Biosensors”, Molecular Biotechnology, Volume 14, Number 2, 109-129, DOI: 10.1385/MB:14:2:109, 2000

[5] Paul D’Orazio, “Biosensors In Clinical Chemistry”, Clinica Chimica Acta 334 (2003) 41–69, 2003

[6] Jonathan M. Cooper and Anthony E.G. Cass, “Biosensors: A Practical Approach”, Oxford University Press, 2004

[7] Edward L. Ciolkowski, Karolyn M. Maness, Paula S. Cahlil, and R. Mark Wightman, Dennls H. Evans, Bruno Fosset, and Christian Amatore, “Disproportionation During Electrooxidation of Catecholamines at Carbon-Fiber Microelectrodes”, Anal. Chem. 1994, 66, 3611-3617

[8] Jian-Wei Mo, Bozidar Ogorevc, “Simultaneous Measurement of Dopamine and Ascorbate at Their Physiological Levels Using Voltammetric Microprobe Based on

Overoxidized Poly(1,2-phenylenediamine)-Coated Carbon Fiber", Anal. Chem. 2001, 73, 1196-1202

[9] N.D. Volkow, J.S. Fowler, G.-J. Wang, and J.M. Swanson, "Dopamine in drug abuse and addiction: results from imaging studies and treatment implications", Molecular Psychiatry (2004) 9, 557–569

[10] C. Scheller, S. Sopper, C. Jassoy, V. ter Meulen, P. Riederer, and E. Koutsilieri, "Dopamine activates HIV in chronically infected T lymphoblasts", Journal of Neural Transmission (2000) 107: 1483–1489

[11] Hari Singh Nalwa, "Handbook of Nanostructured Materials and Nanotechnology", Academic Press, Volume 3, 2000

[12] Abraham P. Lee, James Lee, and Mauro Ferrari, "BioMEMS and Biomedical Nanotechnology", Springer, 2006

[13] M. Meyyappan, "Carbon Nanotubes Science and Applications", CRC Press LLC, 2005

[14] http://www.physorg.com/news193389403.html

[15] Gustavo A. Rivas, María D. Rubianes, María l. Pedano, Nancy F. Ferreyra, Guillermina Luque, and Silvia A.Miscoria, "Carbon Nanotubes: A New Alternative for Electrochemical Sensors", Nova Science Publishers Inc., 2009

[16] http://www.austincc.edu/~emeyerth/elecchem.htm

[17] http://web.iitd.ac.in/~sbasu/ElectrochemistryLectures.pdf

[18] Liao, X. Z.; Serquis, A.; Jia, Q. X.; Peterson, D. E.; Zhu, Y. T.; Xu, H. F.; "Effect of catalyst composition on carbon nanotube growth", Applied Physics Letters, Volume 82, Issue 16, 2694 – 2696, DOI: 10.1063/1.1569655

[19] Young Lee T.; Han J.-H.; Hong Choi S.; Yoo J.-B.; Park C.-Y.; Jung T.; Yu S.; Yi W.K.; Han I.T.; Kim J.M.; "Effects of source gases on the growth of carbon nanotubes", Elsevier, Diamond and Related Materials, Volume 12, Number 3, March 2003 , pp. 851-855(5)

[20] Lahiri I, Lahiri D, Jin S, Agarwal A, and Choi W., "Carbon nanotubes: how strong is their bond with the substrate?", ACS Nano. 2011 Feb 22;5(2):780-7, PMID: 21208010

[21] Cheol Jin Lee, Jeunghee Park, Yoon Huh, and Jeong Yong Lee, "Temperature effect on the growth of carbon nanotubes using thermal chemical vapor deposition", Chemical Physics Letters Volume 343, Issues 1-2, 27 July 2001, Pages 33-38

[22] Y.M. Wong, W.P. Kang, J.L. Davidson, B.K. Choi, W. Hofmeister, and J.H. Huang, " Field emission triode amplifier utilizing aligned carbon nanotubes", Diamond and Related Materials Volume 14, Issues 11-12, November-December 2005, Pages 2069-2073, DOI: 10.1016/j.diamond.2005.09.025

[23] S. Costa, E. Borowiak-Palen, M. Kruszyñska, A. Bachmatiuk, and R J. Kalenczuk, "Characterization of Carbon Nanotubes by Raman spectroscopy", Mater Sci-Poland. (2008), 26, 233-441

[24] Yong Mui Wong, “Fabrication and characterization of carbon nanotubes field emission cathodes grown by CVD with palladium as catalyst”, Thesis (M.S. in Electrical Engineering)--Vanderbilt University, May 2004

[25] Supil Raina, W.P. Kang, and J.L. Davidson, “Nitrogen incorporated nanodiamond film with ‘ridge’ surface morphology for detection of bio-analyte”, Diamond & Related Materials 18 (2009) 574–577, DOI: 10.1016/j.diamond.2008.11.016

[26] Michael E. G. Lyons and Gareth P. Keeley, “The Redox Behaviour of Randomly Dispersed Single Walled Carbon Nanotubes both in the Absence and in the Presence of Adsorbed Glucose Oxidase”, Sensors 2006, 6, 1791-1826

[27] Carrara, Sandro ; Cavallini, Andrea ; De Micheli, Giovanni ; Olivo, Jacopo ; Benini, Luca ; Shumyantseva, Victoria V. ; Arhakov, Alexander I; “Circuits Design and Nano-Structured Electrodes for Drugs Monitoring in Personalized Therapy”, BioCAS 2008, 325-328

[28] Katarína Gmucová , Martin Weis, Drahoslav Barančok, Július Cirák, Pavol Tomčík, and Juraj Pavlásek, “Ion selectivity of a poly(3-pentylmethoxythiophene) LB-layer modified carbon-fiber microelectrode as a consequence of the second order filtering in voltcoulometry”, J. Biochem. Biophys. Methods (2007), Volume 70 Isue 3 385–390, DOI: 10.1016/j.jbbm.2006.09.001

[29] Li Qingwen, Wang Yiming, and Luo Guoan, “Voltammetric separation of dopamine and ascorbic acid with graphite electrodes modified with ultrafine TiO_2”, Materials Science and Engineering: C, Volume 11, Issue 1, 30 June 2000, Pages 71-74, DOI: 10.1016/S0928-4931(00)00132-6

[30] Cheng Fang, Xiaorong Tang, and Xingyao Zhou, “Preparation of Poly(malachite green) Modified Electrode and the Determination of Dopamine and Ascorbic Acid”, Analytical Sciences Vol. 15 (1999) , No. 1 p.41

[31] S. Sharath shankar, B.E. Kumara Swamy, Umesh Chandra, J.G.Manjunatha, and B.S. Sherigara, “Simultaneous Determination of Dopamine, Uric Acid and Ascorbic Acid with CTAB Modified Carbon Paste Electrode”, Int. J. Electrochem. Sci., 4 (2009) 592 - 601

[32] Sara Mahshid, Chengcheng Li, Sahar Sadat Mahshid, Masoud Askari, Abolghasem Dolati, Lixia Yang, Shenglian Luo, and Qingyun Cai, “Sensitive determination of dopamine in the presence of uric acid and ascorbic acid using TiO2 nanotubes modified with Pd, Pt and Au nanoparticles”, Analyst, 2011, 136, 2322-2329, DOI: 10.1039/C1AN15021A

[33] Rong-Sheng Chen, Wei-Hua Huang, Hua Tong, Zong-Li Wang, and Jie-Ke Cheng, “Carbon Fiber Nanoelectrodes Modified by Single-Walled Carbon Nanotubes”, Anal. Chem. 2003, 75, 6341-6345